Numerical Investigation of Aerosol Deposition in Lung Airways During Inhalation and Exhalation

By

Muhammad Farrukh Mehmood

(Registration No: 00000399602)

Department of Mechanical Engineering

School of Mechanical and Manufacturing Engineering

National University of Sciences & Technology (NUST)

Islamabad, Pakistan

(2024)

Numerical Investigation of Aerosol Deposition in Lung Airways During Inhalation and Exhalation

By

Muhammad Farrukh Mehmood

(Registration No: 00000399602)

A thesis submitted to the National University of Sciences and Technology, Islamabad,

in partial fulfillment of the requirements for the degree of

Master of Science in
Mechanical Engineering

Supervisor: Dr. Adnan Munir

School of Mechanical and Manufacturing Engineering

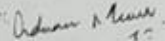National University of Sciences & Technology (NUST)

Islamabad, Pakistan

(2024)

THESIS ACCEPTANCE CERTIFICATE

THESIS ACCEPTANCE CERTIFICATE

Certified that final copy of MS/MPhil thesis written by **Regn No. 00000399602 Muhammad Farrukh Mehmood** of **School of Mechanical & Manufacturing Engineering (SMME)** has been vetted by undersigned, found complete in all respects as per NUST Statues/Regulations, is free of plagiarism, errors, and mistakes and is accepted as partial fulfillment for award of MS/MPhil degree. It is further certified that necessary amendments as pointed out by GEC members of the scholar have also been incorporated in the said thesis titled. **Numerical investigation of aerosol deposition in lung airways during inhalation and exhalation**

Signature:

Name (Supervisor): Adnan Munir

Date: 13 - Feb - 2024

Signature (HOD):

Date: 13 - Feb - 2024
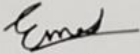
Signature (DEAN):

Date: 13 - Feb - 2024

TH-4 FORM

National University of Sciences & Technology (NUST)
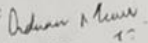
MASTER'S THESIS WORK

We hereby recommend that the dissertation prepared under our supervision by: Muhammad Farrukh Mehmood (00000399602)

Titled: Numerical investigation of aerosol deposition in lung airways during inhalation and exhalation be accepted in partial fulfillment of the requirements for the award of MS in Mechanical Engineering degree.

Examination Committee Members

1. Name: Emad Ud Din   Signature: _____

2. Name: Izhar Ullah   Signature: _____

3. Name: Zeeshan Saeed   Signature: _____

Supervisor: Adnan Munir   Signature: _____

Date: 13 - Feb - 2024

Head of Department

         13 - Feb - 2024

         Date

COUNTERSINGED

13 - Feb - 2024

Date   Dean/Principal

CERTIFICATE OF APPROVAL

This is to certify that the research work presented in this thesis, entitled *During Inhalation*
" Numerical Investigation of Aerosol Deposition in Lung Airways *& Exhalation*
was conducted by Mr./Ms. M. Farrukh Mehmood under the supervision of
Dr. Adnan Munir .

No part of this thesis has been submitted anywhere else for any other degree. This thesis is
submitted to the......................... (Name of Department of the University)................. in
partial fulfillment of the requirements for the degree of Master of Science in Field of
Mechanical Engineering (Subject Name)..
Department of SMME..... National University of Sciences and Technology, Islamabad.

Student Name: _M Farrukh Mehmood_   Signature: _____

Examination Committee:

    a) External Examiner 1: Name   Signature: _____
    (Designation & Office Address)

    ....

    b) External Examiner 2: Name   Signature: _____
    (Designation & Office Address)

    ....

Supervisor Name: Dr. Adnan Munir   Signature: _____

Name of Dean/HOD: Dr. Mian Ashfaq Ali   Signature: _____

AUTHOR'S DECLARATION

I <u>Muhammad Farrukh Mehmood</u> hereby state that my MS thesis titled "<u>Numerical Investigation of Aerosol Deposition in Lung Airways During Inhalation and Exhalation</u>" is my own work and has not been submitted previously by me for taking any degree from National University of Sciences and Technology, Islamabad or anywhere else in the country/ world.

At any time if my statement is found to be incorrect even after I graduate, the university has the right to withdraw my MS degree.

Name of Student: <u>Muhammad Farrukh Mehmood</u>

Date: <u>14-02-2024</u>

PLAGIARISM UNDERTAKING

I solemnly declare that research work presented in the thesis titled "**Numerical Investigation of Aerosol Deposition in Lung Airways During Inhalation and Exhalation**" is solely my research work with no significant contribution from any other person. Small contribution/ help wherever taken has been duly acknowledged and that complete thesis has been written by me.

I understand the zero tolerance policy of the HEC and National University of Sciences and Technology (NUST), Islamabad towards plagiarism. Therefore, I as an author of the above titled thesis declare that no portion of my thesis has been plagiarized and any material used as reference is properly referred/cited.

I undertake that if I am found guilty of any formal plagiarism in the above titled thesis even after award of MS degree, the University reserves the rights to withdraw/revoke my MS degree and that HEC and NUST, Islamabad has the right to publish my name on the HEC/University website on which names of students are placed who submitted plagiarized thesis.

Student Signature: _____

Name: Muhammad Farrukh Mehmood

DEDICATION

Dedicated to my exceptional parents, supportive spouse, and adored siblings whose tremendous support and cooperation led me to this wonderful accomplishment.

ACKNOWLEDGEMENTS

I would like to begin by expressing my heartfelt gratitude to Allah Subhanahu Wa Ta'ala, my Creator, for His continuous guidance and blessings throughout the duration of this work. Without His unwavering support and the inspiration, He has bestowed upon me, I would not have been able to enhance my research. All praise and thanks are solely due to Allah Subhan Tallah.

I feel great pleasure in extending my heartfelt gratitude to my supervisor, Dr. Adnan Munir, for his tireless efforts and continuous motivation. I would also like to thank Dr. Emad Uddin and Dr. Izhar Ullah for being part of my thesis guidance and evaluation committee.

I would like to express my sincere appreciation to my parents for their constant love, support, and unwavering belief in my abilities. They have been my pillars of strength, providing guidance and encouragement at every step of my academic pursuits.

I am also immensely grateful to Umar Farooq, Hafiz Hamza Riaz, and Attique Arshad, my fellow colleagues in the Microfluidics lab, for their invaluable assistance and unwavering support in resolving problems related to computational analysis. Their expertise and availability whenever I faced challenges have been indispensable to the successful completion of my thesis. I deeply appreciate their dedication and assistance throughout this research journey.

Finally, I extend my thanks to all the individuals who have helped me throughout my study. Their contributions, whether big or small, have played a significant role in the successful completion of my thesis.

TABLE OF CONTENTS

LIST OF TABLES

LIST OF FIGURES

LIST OF SYMBOLS, ABBREVIATIONS AND ACRONYMS

GD   Grain Dust

CFA   Coal Fly Ash

BC   Bituminous Coal

G3   Lung Airway Generation 3

G4   Lung Airway Generation 4

SS   Sedentary State

LA   Light Activity

MA   Moderate Activity

VA   Vigorous Activity

ABSTRACT

Continuous deposition of workplace pollutant particles on lung airways during respiratory actions seriously threatens the lung health of persons performing tasks in polluted environments. While inhalation-deposition relationships have been explored, the impact of exhalation on the deposition of polydisperse particles remains unclear. This study aims to analyze the exhalation-driven deposition of fine and coarse occupational pollutant particles in polydisperse form, considering varying levels of physical activity. Computer simulations are conducted on the airway section G3-G4 to study the patterns of airflow dynamics and deposition of grain dust, coal fly ash, and bituminous coal particles across a spectrum of activity intensities, utilizing idealized and realistic lung models. Key findings include the observation of early emergence of secondary flows in the real model compared to the idealized model, a notable shift in deposition patterns towards the post-bifurcation zones, and the influence of physical activity intensity on particle deposition. Additionally, deposition primarily occurs near the cranial ridge during inhalation, while exhalation leads to deposition in pre- and post-bifurcation zones. The effect of gravity on deposition is more pronounced at lower flow rates but diminishes at higher flow rates. PM2.5 deposition is

minimal and random in the idealized model but becomes more significant and consistent in the real model, with substantial deposition rates observed for PM10 particles. This research underscores the increased risk of lung diseases for workers in polluted environments during vigorous activity.

CHAPTER 1: INTRODUCTION

The Industrial Revolution instigated an era where the atmosphere is progressively overtaken by a variety of dangerous. At present, roughly 99 percent of the globe's population resides in places where air pollution levels are higher than acceptable levels, leading to the startling fact that over seven million premature deaths are caused by air pollution annually(World Health Organization, 2023).

Every time they breathe in, most people unintentionally take in a significant number of airborne pollutants. These tiny particles, which can range from harmful gases produced from combustion sources to small particulate matter exhaled by automobiles and industrial activities, enter the sensitive respiratory tissues with frightening ease. Not only does this continuous exposure to airborne pollutants impair lung function, but there are also health concerns to the body as a whole since these toxic compounds may enter the circulation and damage important organs all throughout the body. In addition, occupational pollution has become a grave concern that causes lung cancer and cardiovascular diseases [2].

Paul et al.'s [3] inquiry uncovered a startling fact: coal worker's pneumoconiosis (CWP), which is brought on by breathing in coal dust, was the cause of 18.3% of miners' fatalities. The dangerous work dangers that miners face is highlighted by this discovery. There is a serious risk to respiratory health with every breath in the dusty coal mine environment. The well-being of coal miners is at risk, and these numbers highlight the urgent need for strict safety procedures and vigilant health monitoring. According to studies by [4] and [5] a concerning finding is that a large number of employees at grain processing facilities have asthma caused by grains. Their respiratory health is gravely endangered by breathing in grain dust, which is full of allergens and irritants, all day long. The symptoms can be rather difficult to manage, including wheezing to asthma. Consequently, it is imperative that these establishments intensify their safety protocols and closely monitor the well-being of their employees.

The residual product identified as coal fly ash (CFA) from thermal power plants is widely used in the making of bricks, according to [6] However, as [7] point out, individuals

in CFA-related operations encounter severe health risks since CFA contains carcinogenic ingredients including lead and arsenic. This emphasizes how important it is for CFA-using industries to have strict occupational health and safety policies in place to safeguard employees from potentially harmful compounds and related health hazards.

1.1 Literature Review

Pollution from coal mines (CM), grain processing facilities (GPF), and the coal fly ash brick industry (CFBI) is referred to as "particulate matter (PM)" pollution. This has been reported by [8], [9], [10] .This phrase refers to the wide range of airborne particles that are released during industrial activities within various industries, from fine dust and soot to aerosols. It is critical to acknowledge the widespread presence of PM pollution in various sectors in order to comprehend the complex issues that airborne pollutants present and to develop practical mitigation techniques that will protect the environment and human health.

The difference between PM2.5 and PM10, as described by [11], is critical when it comes to particulate matter (PM) pollution. PM2.5 is a class of tiny particles that have a diameter of less than 2.5 micrometers. These particles have the potential to severely penetrate the respiratory system and pose serious health hazards. PM10, on the other hand, is classified as coarse PM and includes particles that range in size from 2.5 to 10 micrometers. Researchers can identify the ways in which fine and coarse PM impact human health and develop focused approaches to lessen their negative impacts on public health by gaining a grasp of these particles' properties.

Particles like PM2.5 and PM10 are taken into the lungs while breathing and land on different parts of the lung airways, as research by [12] and [13] has demonstrated. Particles deposited in the respiratory system may have a significant impact on lung health, perhaps causing respiratory discomfort, inflammation, and chronic respiratory conditions. Knowing the kinetics of particle deposition in the lungs is essential to understanding the processes that underlie the detrimental health impacts of exposure to air pollution. This

kind of information is essential for shaping healthcare initiatives meant to reduce the respiratory hazards associated with airborne particulate matter.

Extensive research has been conducted by [14] and [15] to show that lung disorders caused by exposure to PM2.5 and PM10 are associated with higher death rates. These data highlight the serious effects of breathing in airborne particulate matter over extended periods of time since high concentrations of PM2.5 and PM10 greatly increase the risk of respiratory diseases and the death that goes along with them. This research has important ramifications that highlight the pressing need for effective public health initiatives to protect the respiratory health of impacted communities and lower ambient particulate matter levels.

According to [16], there is an increased risk of pollutant particle absorption and deposition in the lung airways when physical activity (PA) is performed in particulate matter-polluted working settings. This finding emphasizes how intricately individual behaviors and occupational exposures interact, with deeper breathing and faster breathing rates during physical activity leading to a higher intake of airborne contaminants. As a result, there is an increase in the accumulation of these particles in the respiratory system, which may put workers who are exposed to particulate matter pollution at risk for respiratory illnesses. Comprehending the mutual benefits of physical exercise and environmental contaminants is essential for enhancing workplace safety measures and reducing the detrimental impacts of occupational exposures on health.

As [17] point out, there is still much to learn about the complex interaction between the degree of physical activity in different contaminated settings and the deposition of particles. We still don't fully grasp how varying degrees of physical activity affect how airborne contaminants deposit in the respiratory system. This is despite great strides in study. The intricacy of environmental health dynamics is highlighted by this ambiguity, as a multitude of elements, such as pollutant properties, personal physiological reactions, and environmental circumstances, combine to influence the accumulation and consequent health impacts of inhaled particles. In order to minimize the detrimental effects of particulate matter pollution on respiratory health and to improve our understanding of

3

occupational and environmental health concerns, it is critical that this information gap be closed.

Most research examining the impact of particulate matter on lung health focuses on inhalation mechanisms. An important statistic is particle deposition efficiency (DE), which shows the percentage of particles deposited in the respiratory system compared to the total number of particles injected into the system. Notably, deposition efficiency shows an increasing tendency with increasing particle sizes and intensities of physical activity, especially in the trachea and the first three generations (G1–G3) of airway branching [18]. This association highlights how important it is to take into account both individual physiological responses and particle features when evaluating inhaled pollutant deposition patterns and their possible effects on respiratory health.

There is a similar pattern of deposition efficiency in the airway generations G3–G5, which is documented in tandem with the trachea and beginning generations. [19] have explained that there is a noteworthy anomaly in the lower airways, particularly in generations G14-G16, where deposition efficiency exhibits a declining tendency with increasing physical activity intensity. This difference emphasizes the intricate relationships between physical activity levels and the kinetics of particle deposition across the respiratory tract, highlighting the intricacy of these interactions with environmental health across several anatomical locations. These kinds of discoveries are extremely helpful in explaining the complex processes that underlie the deposition of particles in the lungs and in providing tailored therapies to lessen the harmful effects of airborne pollution exposure on respiratory health.

Research regarding the influence of exhalation on the deposition of these particles during various levels of PA is rare. In an experimental study on exhalation, [20] found deposition hot spots in the pre-bifurcation zone of G3-G4 and attributed this phenomenon to the vortices generated by the secondary flows. [21] also found similar patterns of deposition hotspots in their numerical study on particle deposition in expiratory flow. [22] observed the correlation between particle deposition during exhalation and Dean number (D) and found the deposition efficiency to increase when D>100 at a constant Stokes

number. All these researchers relied on idealized airway structure. Given the intricacy brought about by variances in airway anatomy among people, the necessity for study on real geometries becomes clear. While real geometries have been investigated in inhalation studies[23], [24], [25], there is a significant void in the literature for exhalation-related research.

Pollutant particles are found with a wide range of diameters. However, most of the researchers have focused on monodispersed deposition in their studies. Only a few studies analyzed polydisperse particle deposition [26]. [27] studied the effect of the density and particle size along with polydispersity on the DE and found that large but light particles deposited less than tiny but dense particles. However, the difference in deposition efficiencies becomes less prominent with an increase in median diameter. In a comparison performed by [28], the deposition efficiency (DE) of polydisperse particles was higher than that of monodisperse particles. Turbulence effects on the deposition of large-size particles are found to be higher than on small-size particles in a polydisperse transport and deposition (TD) study [29]. All these researchers considered inhalation to study the polydisperse deposition. No existing studies have examined the influence of polydispersity on aerosol deposition in bronchial airways during exhalation.

1.2 Research Motivation

This research was motivated by the pressing need to understand and mitigate the health risks associated with working in locations where air pollution is present. Workers in many different industries, such as manufacturing, construction, and mining, regularly encounter high quantities of airborne particles that might damage their respiratory systems. Grain dust, coal fly ash, and bituminous coal are some of these particles. We still don't fully understand how these pollutants affect lung health at different intensities of physical exercise. This study attempts to close this information gap by examining the patterns of fine (PM2.5) and coarse (PM10) polydisperse particle deposition in the airways during exhalation. It is essential to comprehend how different physical activity levels affect the amount of pollutant particles deposited to develop measures that effectively safeguard workers' health and reduce occupational dangers. Furthermore, contrasting the deposition

behaviors in realistic and idealized lung models sheds light on how complicated anatomy affects particle deposition.

Ultimately, by offering a thorough grasp of the variables driving particle deposition in the respiratory system, this research hopes to make a significant contribution to occupational health. These discoveries can lead the creation of focused treatments and occupational safety regulations to protect the health of employees exposed to airborne contaminants.

1.3 Research Aim

This study aims to investigate the polydisperse deposition of pollutant particles on the G3-G4 pulmonary airways in the context of workplace pollution under four levels of physical activities: sedentary state (SS), light activity (LA), moderate activity (MA), and vigorous activity (VA).

1.4 Research Objectives

The goal of the study is to investigate the intricate dynamics of particle deposition inside the respiratory system, with a focus on the airway segment G3–G4. The primary objective is to investigate the effects of varying levels of physical activity on the patterns of fine (PM2.5) and coarse (PM10) polydisperse particle deposition during expiration. Additionally, the study looks at how different types of pollution particles, such grain dust, coal fly ash, and bituminous coal, influence how they settle in the airways. A comparative investigation will be performed to ascertain the relative impacts of mono and polydisperse particles on respiratory particle deposition. Moreover, the study will also assess the importance of anatomical details by contrasting deposition patterns in idealized and realistic lung models.

1.5 Hypothesis

Building on the insights gained from the literature analysis, a hypothesis can be formulated that considering particle polydispersity and expiratory flow, the deposition of polydisperse particles during exhalation is higher compared to monodisperse particles.

CHAPTER 2 METHODOLOGY

2.1 Airway Geometry

Lung airway generations G3-G4 are selected because the numerical model can be tested at these generations using the available experimental data [20]. Both the ideal and real lung models will be analyzed and a comparison between the two scenarios will be provided. This study is focused on the deposition mechanisms only at one bifurcation of human lung airways instead of the deposition in a complex human lung. Typically, airway G3 is vertically aligned and parallel to the gravity direction defined as **g** parallel to G3. However, work activities may involve bending or lying positions of body, making the gravity direction **g** perpendicular to all the G3-G4 airways as indicated in Figure 2c. As the sedimentation due to gravity enhances particle deposition, the considered configuration is shown in Figure 2c to examine the maximum possible deposition rates.

2.1.1 Realistic Model of Airways G3-G4

The study makes use of lung CT-scanned DICOM pictures of an adult 55 years of age that were obtained from a nearby hospital. Key anatomical components including the trachea and the first four lung generations (G0-G4) are carefully included into a meticulously constructed three-dimensional model of the lung using geometry modeling software. This work explores the complexities of particle deposition in these airway branches, with a particular focus on a stretch that spans generations G3 to G4. Through close examination of this focused area, the study seeks to offer a thorough grasp of deposition trends and their effects on respiratory health. With its ability to facilitate a detailed investigation of the dynamics of pollutant exposure in the human respiratory system, this method makes significant contributions to the fields of respiratory physiology and environmental health. For the present study, a segment of the lung model spanning generations G3 to G4 is extracted (Figure 2.1).
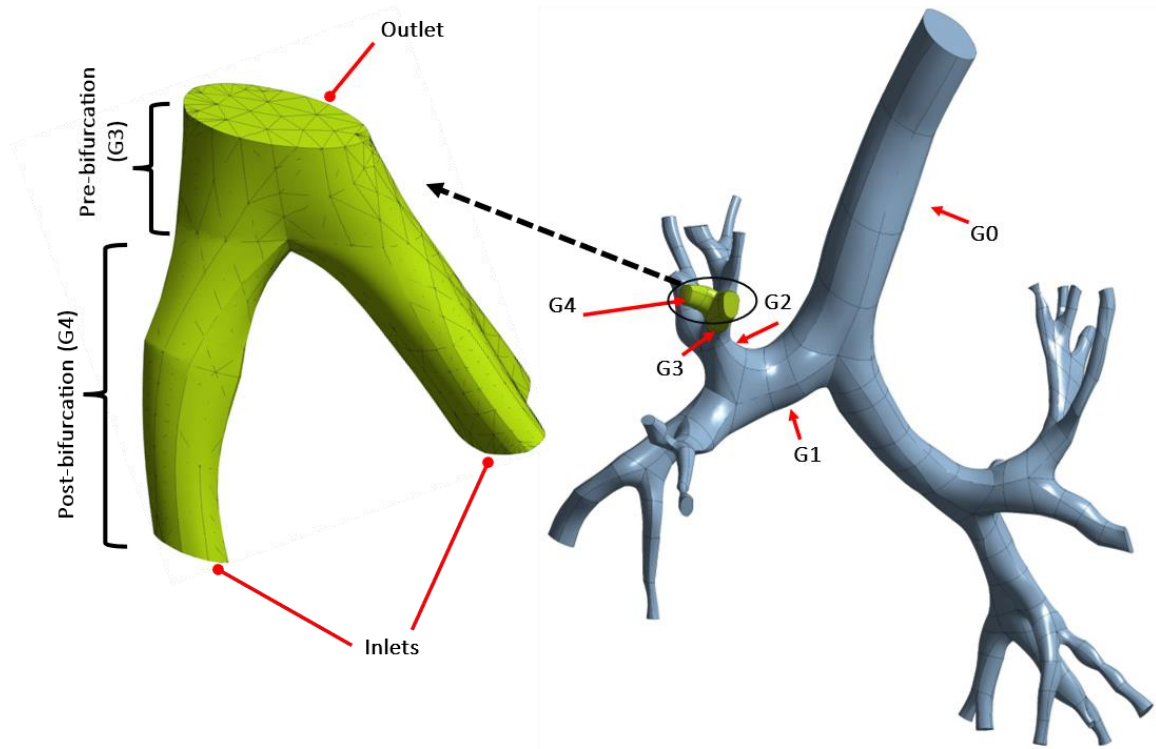
Figure 2. 1: Real lung model: (Right) CT-scanned lung model encompassing the trachea to generation 4; (Left) Extracted segment showing generations 3 and 4.

2.1.2 Idealized Model of Airways G3-G4

The idealized 3D model of G3-G4 airways is constructed by taking the dimensions as per the experimental model of [20]. The diameters of G3 and G4 airways are 0.5 cm and 0.4 cm, respectively [30], and the respective lengths are 10 cm and 5 cm, respectively. The point of bifurcation is defined as the point where the G3 airway splits into two parts. The focus of the analysis is between the region 2.5 cm before the bifurcation point and 2.5 cm after the bifurcation point as indicated in the colored part in Figure 2.2b. The region is sub-divided (as seen in Figure 2.2b, c.) into two zones: Pre-bifurcation zone and post-bifurcation zone, in correspondence with sections C and D of experimental model of [20].
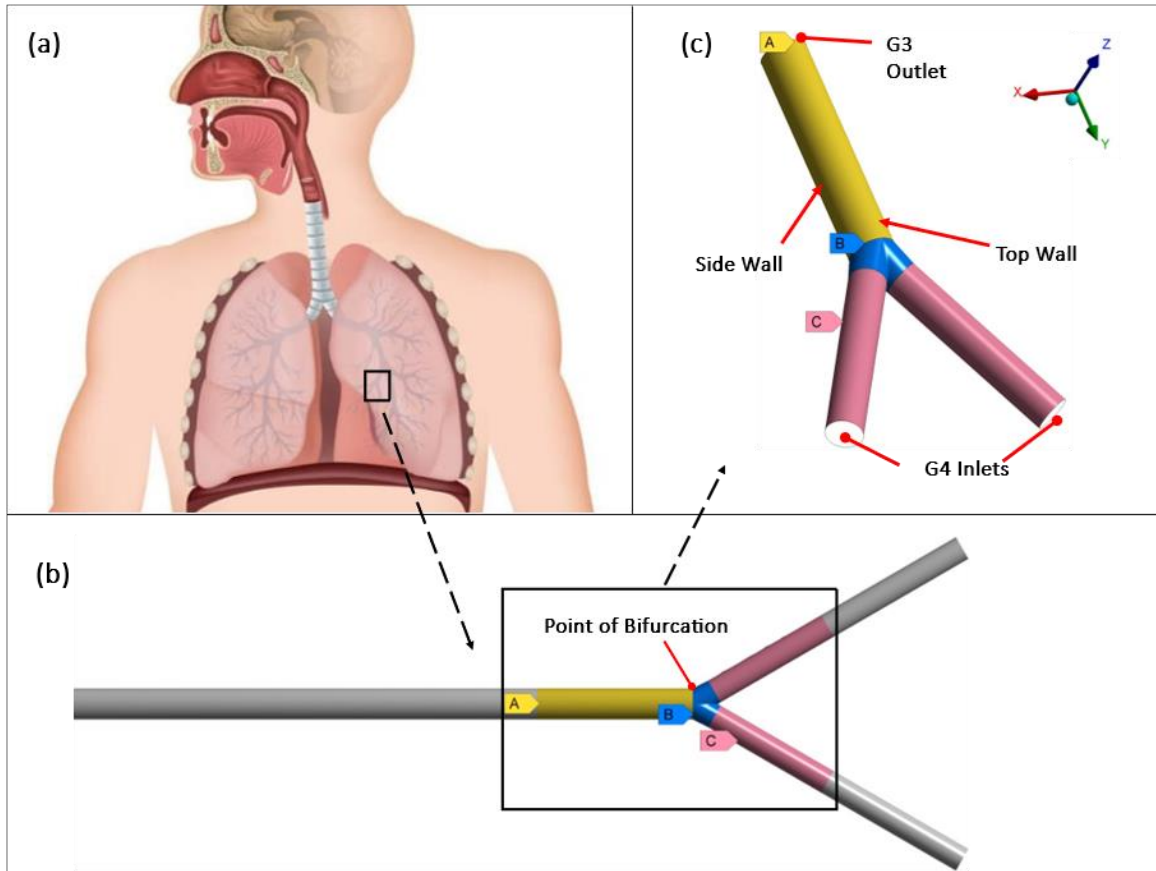
Figure 2. 2: (b): Schematic diagram of G3-G4. Colored section 'A' represents pre-bifurcation zone and sections 'B', and 'C' post-bifurcation zone. (c): The orientation of G3-G4 human lung airway with inlets, outlet, top and side walls indicated.

2.2 Governing Equations

The numerical investigation of aerosol deposition in lung airways during inhalation and exhalation involves solving a set of governing equations using computational fluid dynamics. These equations are essential in understanding the behavior of the aerosol particles and their distribution within the respiratory system.

2.2.1 Airflow Equations

The Reynolds-averaged Navier-Stokes equations are used to model turbulent fluid flow. They involve averaging the governing equations over time to simulate complex and chaotic behaviour. Turbulence models are used to approximate the effects of turbulent

10

fluctuations. RANS equations are widely used in engineering for predicting and analyzing various flow phenomena. The continuity equation along with RANS equations are given in equations (2.1) and (2.2) respectively.

$$\frac{\partial \rho}{\partial t} + \frac{\partial}{\partial x_i}(\rho u_i) = 0 \tag{2.1}$$

$$\frac{\partial}{\partial t}(\rho u_i) + \frac{\partial}{\partial x_j}(\rho u_i u_j) = -\frac{\partial p}{\partial x_i} + \frac{\partial}{\partial x_j}\left[\mu\left(\frac{\partial u_i}{\partial x_j} + \frac{\partial u_j}{\partial x_i}\right)\right] + \frac{\partial}{\partial x_j}\left(-\rho\overline{u_i'u_j'}\right) \tag{2.2}$$

where i ranges from 1 to 3, $(x_1, x_2, x_3) = (x, y, z)$, ρ and μ are the density and molecular viscosity of air respectively, g is the gravitational acceleration in the z-direction, and 'u_i' represents the three-dimensional velocity in the x_i-direction and $-\rho\overline{u_i'u_j'}$ is Reynolds stress term which is given as:

$$-\rho\overline{u_i'u_j'} = \mu_t\left(\frac{\partial u_i}{\partial x_j} + \frac{\partial u_j}{\partial x_i} - \frac{2}{3}\frac{\partial u_k}{\partial x_k}\delta_{ij}\right) - \frac{2}{3}\rho k\delta_{ij} \tag{2.3}$$

where μ_t represents turbulent eddy viscosity.

Shear Stress Transport (SST) k-ω model is used to solve turbulent eddy viscosity. The SST k-ω model is a widely used turbulence model in computational fluid dynamics (CFD) simulations. It combines the advantages of both the k-ε and k-ω models to accurately capture turbulence behavior in a wide range of flow conditions. It has the ability to accurately predict shear stresses in boundary layers. By solving transport equations for turbulence kinetic energy (k) and specific dissipation rate (ω), the SST k-ω model provides improved accuracy and robustness compared to other turbulence models. It is a popular choice for simulating complex flows in engineering applications. It needs to solve two equations: one is for turbulent kinetic energy and the other one is for solving turbulence dissipation rate. Both the equations are as follows:

$$\frac{\partial}{\partial t}(\rho k) + \frac{\partial}{\partial x_1}(\rho k u_1) = \frac{\partial}{\partial x_2}\left(\Gamma_k \frac{\partial k}{\partial x_2}\right) + \tilde{G}_k - Y_k + S_k \tag{2.4}$$

$$\frac{\partial}{\partial t}(\rho \omega) + \frac{\partial}{\partial x_1}(\rho \omega u_1) = \frac{\partial}{\partial x_2}\left(\Gamma_\omega \frac{\partial \omega}{\partial x_2}\right) + \tilde{G}_\omega - Y_\omega + D_\omega + S_\omega \tag{2.5}$$

2.2.2 Equations for Particle Motion Dynamics

The deposition mechanisms for fine and coarse are primarily gravitational sedimentation and inertial impaction [25], [31]. The numerical model includes Euler-Lagrange approach with one way coupling. The path of particles is governed by the following force balance equations:

$$m_p \frac{d\boldsymbol{u}^p}{dt} = \boldsymbol{F}_{body} + \boldsymbol{F}_{surface} \tag{2.6}$$

$$\boldsymbol{F}_{body} = \boldsymbol{F}_{gravitational} = m_p \frac{(\rho_p - \rho)}{\rho}\boldsymbol{g} \tag{2.7}$$

$\boldsymbol{F}_{body}$ is the gravitational force given as and $\boldsymbol{F}_{surface}$ is composed of drag force and Saffman lift force.

$$\boldsymbol{F}_{surface} = \boldsymbol{F}_{drag} + \boldsymbol{F}_{saffman} \tag{2.8}$$

$$\boldsymbol{F}_{drag} = m_p \frac{\boldsymbol{u} - \boldsymbol{u}_p}{\tau} \tag{2.9}$$

where τ is the particle relaxation time which is given as[32]

$$\tau = \frac{4\rho_p d_p^2}{3\mu C_d Re} \tag{2.10}$$

here C_d is the drag cofficient and Re is the relative reynolds number given as

12

$$Re = \frac{\rho d_p}{\mu}|\boldsymbol{u}_p - \boldsymbol{u}| \tag{2.11}$$

Saffman's Lift force is given as[33], [34]

$$\boldsymbol{F}_{Saffman} = m_p \frac{2K\nu^{\frac{1}{2}}\rho d_{ij}(\boldsymbol{u} - \boldsymbol{u}_p)}{\rho_p d_p (d_{lk}d_{kl})^{\frac{1}{4}}} \tag{2.13}$$

where $d_{ij} = \frac{1}{2}(u_{i,j} + u_{j,i})$ is the deformation tensor and K=2.594.

According to this distribution method, mass fraction of particles greater than a diameter d, as shown in Figure 2.3, is given by following equation [35]:

$$Y_d = e^{-\left(\frac{d}{\bar{d}}\right)^n} \tag{2.14}$$

where $\bar{d}$ is size constant with a value of 1.75 µm for PM2.5 and 6.5 µm for PM10 and n is the spread parameter, with a value of 3.5.
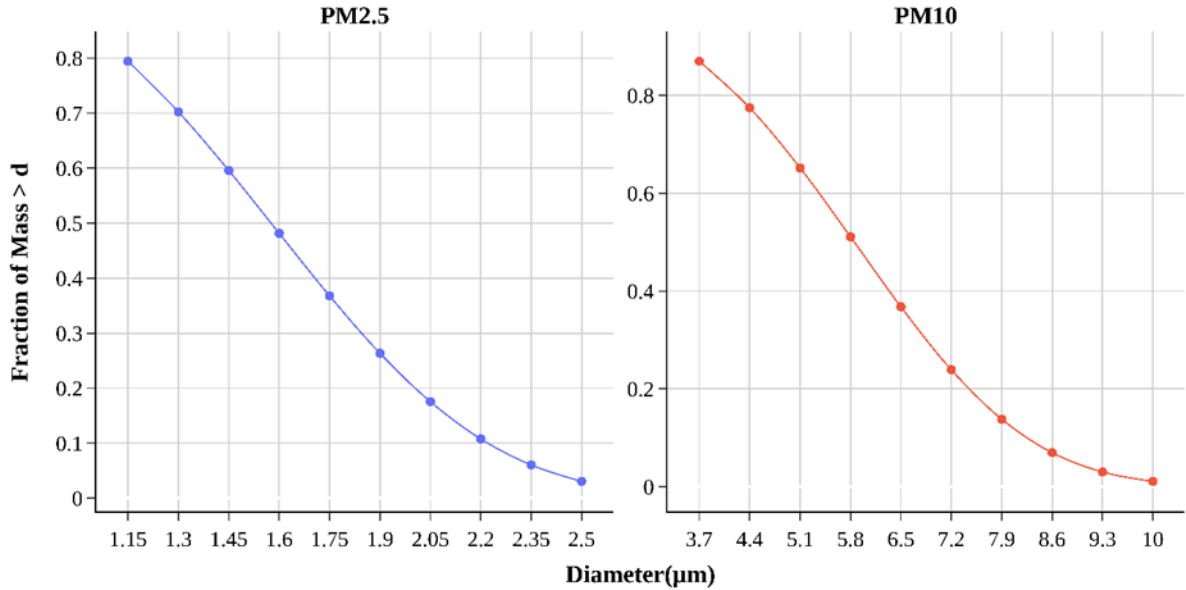

Figure 2. 3: Initial mass distribution of polydisperse particles

13

2.2.3 Deposition Efficiency

The deposition fraction is analyzed in two ways:

1. Deposition of individual particles diameters based on their initial distribution.

$$DE_i = \frac{N_{trap,i}}{N_{inj,i}} \times 100 \tag{2.15}$$

2. Total deposition which refers to the cumulative deposition of particles of all diameters.

$$DE_{total} = \frac{\sum_{i=1}^{n} N_{trap,i}}{\sum_{i=1}^{n} N_{inj,i}} \times 100 \tag{2.16}$$

where $N_{inj,I}$ and $N_{trap,i}$ represent the number of particles of a diameter i injected into the system and trapped in the system respectively

2.3 Solver Setting

ANSYS Fluent is used to conduct numerical analysis. The flow is assumed to be incompressible and transient. The solver solves the Reynolds Averaged Navier-Stokes (RANS) equations to simulate the air flow in the computational domain.

2.3.1 Airflow and Particle Dynamics Settings

In ANSYS Fluent, Shear Stress Transport (SST) k-ω model is used to solve turbulent eddy viscosity. Pressure-based solver is opted to compute the incompressible flow. To simulate the motion of the particles in the Lagrangian scheme and airflow in the Eulerian scheme, the Dense Discrete Phase Model (DDPM) is used with implicit formulation. The Phase Coupled SIMPLE method is employed for pressure-velocity coupling while the first-order upwind scheme is used for the spatial discretization of momentum, volume fraction, and turbulent kinetic energy. To solve pressure, the PRESTO scheme is used. To model the turbulent dispersion of particles, Stochastic Tracking method is used with Discrete

Random Walk Models (DRWM) enabled. Random Eddy Lifetime (REL) method is employed to randomize the characteristic lifetime of eddies.

The exact number of particles that enters G-4 during exhalation cannot be known without a whole lung analysis (Inthavong et al., 2010). The numbers of 44730 and 61040 particles for ideal and real lung geometries, respectively, are chosen based on particle independence tests. The diameters chosen for the study range from 1.15 µm to 2.5 µm for PM2.5 and from 3.7 µm to 10µm for PM10.

2.3.2 Boundary Conditions

During exhalation, the air enters the lung model reversely at the two inlets of G4, where the velocity is given, and particles are released in the numerical simulations. The model walls are set with trap boundary conditions for particles while the outlet face is specified with an escape boundary condition. Air flow Reynolds numbers at the inlets of idealized G4 are taken as 332, 664, 994, and 1327, corresponding to the tracheal outflows of 15 lpm, 30 lpm, 45 lpm, and 60 lpm. Particles are injected with surface injection setup. Initial velocity of the particles is kept the same as the velocity of air entering G4.

2.4 Mesh Independence

The computational domains of real and ideal lung models are discretized in unstructured and structured meshes respectively with 7 and 25 respective inflation layers near the airway walls (Figures. 2.4, 2.5). Mesh independence tests are performed by implementing the numerical model discussed above on 5 different meshes from coarse to fine with 5 µm particle and tracheal flow rate of 8 l/min. The difference between deposition efficiencies with the last two meshes is close to 0% in both the cases. Thus, the benchmark for mesh independence is achieved and meshes consisting of 580307 elements for real geometry and 580773 elements for ideal geometry (2nd last meshes) have been for further analyses. Results of mesh independence tests are presented in Figure. 2.6.

2.5 Model Validation

For model validation, simulations are conducted by taking the geometric dimensions and the parameters same as used in the experimental study of [20]. These parameters are listed in Table 2.1. Figure 2.7 demonstrates excellent agreement between the simulated and experimentally measured deposition rates for different particle sizes during exhalation. Hence, the numerical model employed in the current study can predict highly accurate results of deposition efficiencies of various particle sizes in the upper lung generations during exhalation.
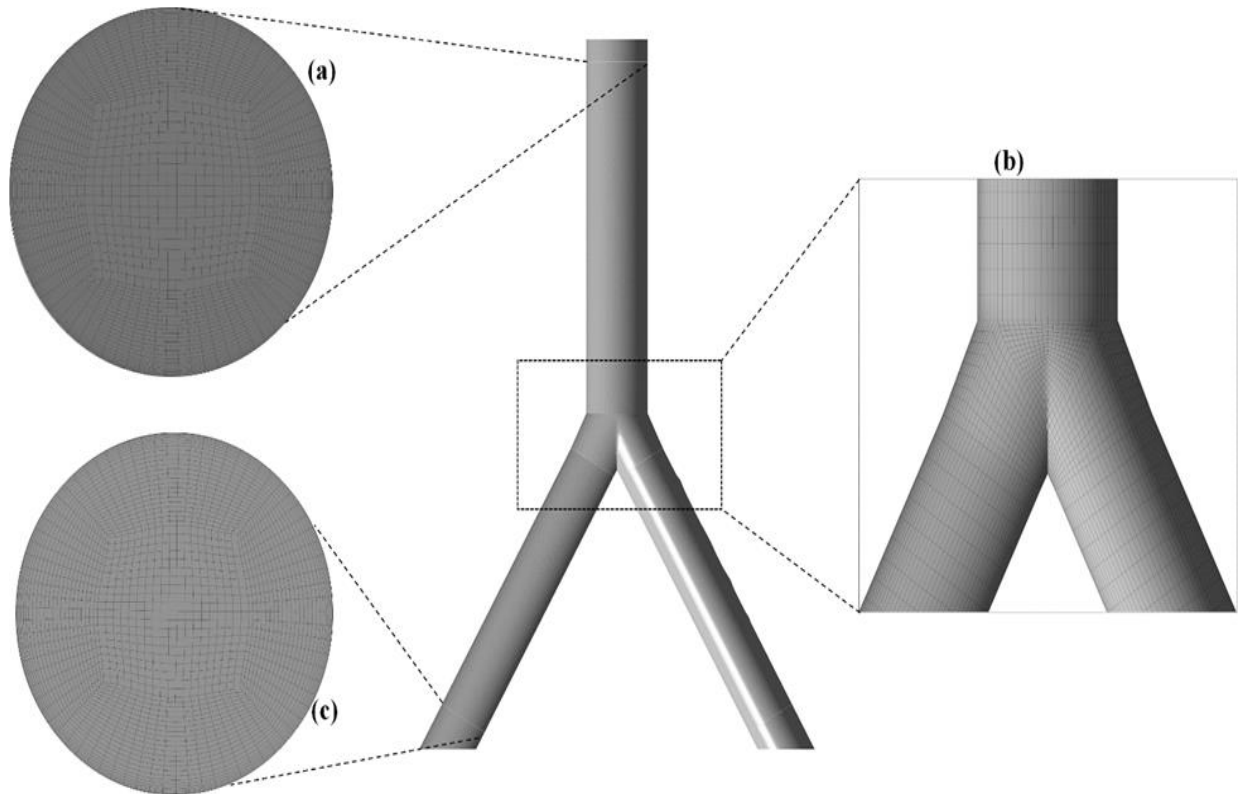

Figure 2. 4: Structured mesh representation of the ideal model for G3-G4 with 25 inflation layers: (a) Outlet mesh, (b) Mesh in the vicinity of the bifurcation, and (c) Inlet mesh.
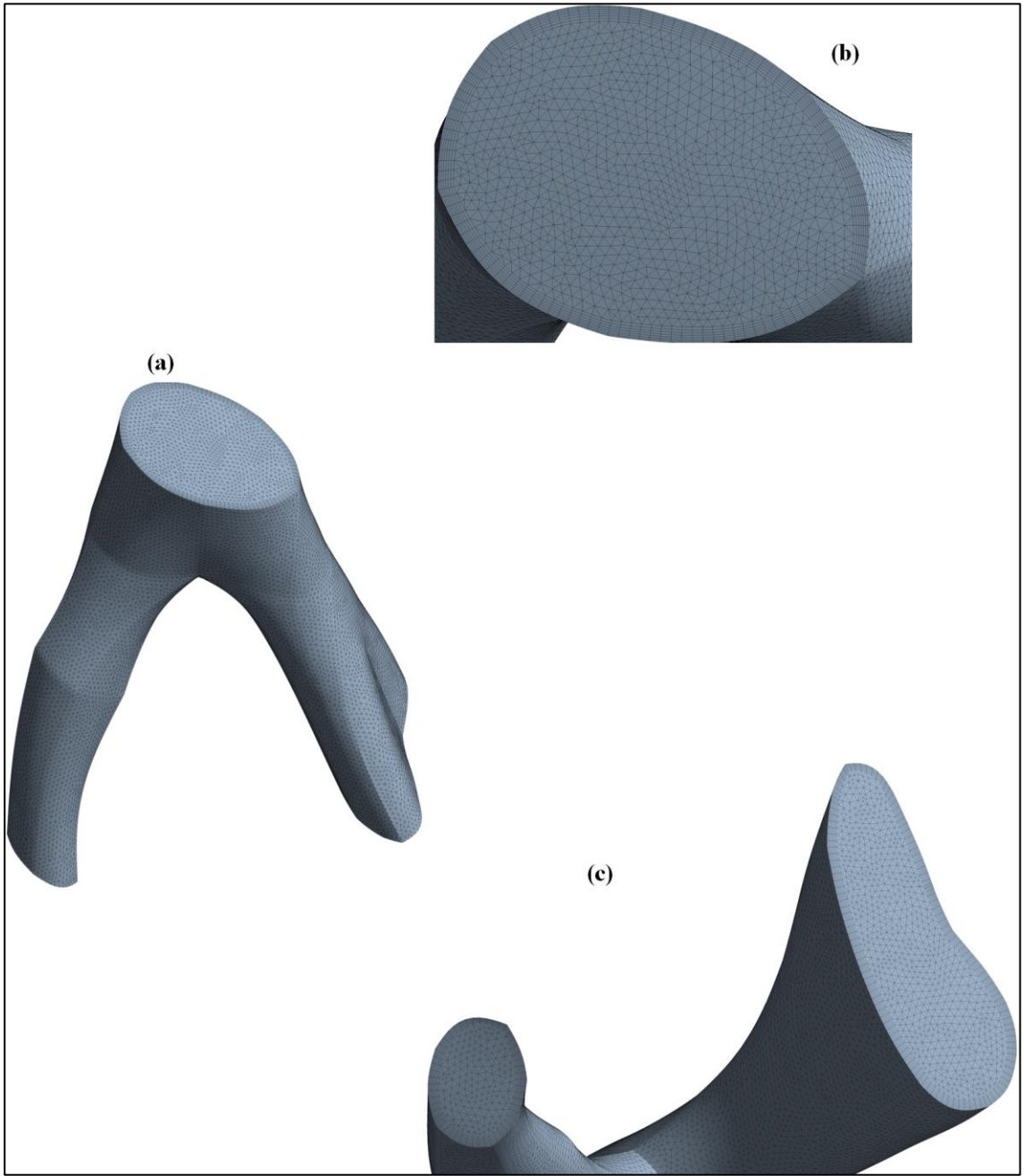
Figure 2. 5: Unstructured mesh representation of the G3-G4 real geometry model with 7 inflation layers: (a) Full model mesh, (b) Outlet mesh, and (c) Inlet mesh.

Table 2.1: Parameter values taken from KIM et al., [20] for the model validation.

Parameter	Value
Particle material	Olefin acid
Particle Density (kg/m^3)	891
Flow rates at parent branch (l/min)	4, 6, 8, 12, 16, 21
Particle diameter (μm)	3, 5, 7

Figure 2. 6: Results of mesh independence tests conducted with the particles of 5 µm diameter are depicted in (a) for ideal model mesh and (b) for real model mesh.

Figure 2. 7: Validation of numerical model against the experimental data of KIM et al. [36].

CHAPTER 3: RESULTS AND DISCUSSION

During inhalation, inertial impaction is responsible for large amount of deposition at sharp cranial ridge of bifurcation zo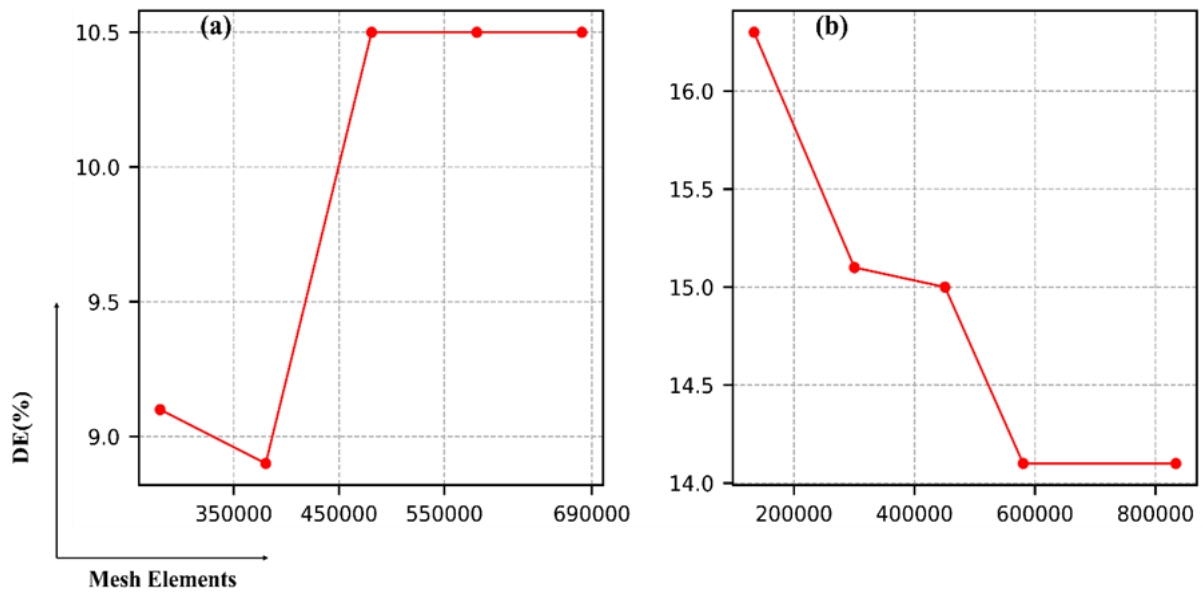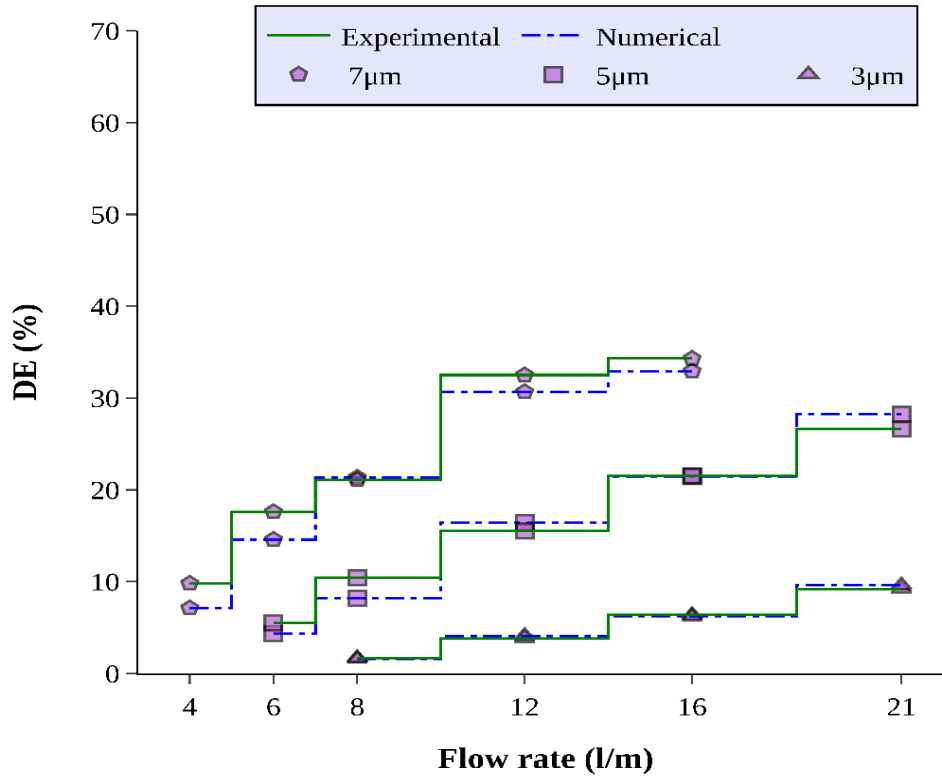ne [20], [31]. However, such a hurdle for airflow is not present during exhalation, therefore, inertial impaction mechanism is not dominant in exhalation and most of the deposition is caused by vortices generated by secondary flows. This deposition occurs mostly at walls of pre and post bifurcation zones. The cranial ridge receives only a small chunk of deposition [20], [21].

3.1 Airflow Analysis

3.1.1 Idealized Lung Model

Reynolds numbers (Re) corresponding to tracheal outflows of 15 l/m and 60 l/m are found to be 550 and 2035 respectively at the bifurcation point of G3-G4, and 644 and 2245 respectively at the outlet of G3. Patterns of turbulent kinetic energy (TKE) normalized with respect to inlet flow velocities are shown in Figure 8 as a measure of the turbulence formation in G3-G4. Flow in G4 remains laminar for all the flow rates. At the outlet of G3, Re gains a maximum value of 644 at 15 l/min flow rate which indicates that at lower flow rates, flow remains laminar in G3 (Figure 3.1a). However, at flow rate of 60 l/m, flow becomes transitional down stream of cranial ridge in G3 because Re varies from 2035 to 2245 (Figure 3.1b).

Figures. 3.2, 3.3 show the characteristics of airflow in idealized G3-G4 under the tracheal flow rates of 15 l/m and 60 l/m on some sections near the bifurcation. Secondary flows develop as the air passes through the bend section of a tube (Pradhan & Guha, 2019). In present case, these flows are developed in the bifurcation zone. As a result, second-flow vortices are formed near the cranial ridge and their strength reduces as they move downstream, but are still visible near the exit and section D. These vortices are initially generated near the top and bottom walls of the G3 (cross-sections A, Figures. 3.2, 3.3). Their centres move towards the centre of the tube and form a four-vortex flow structure at

cross-sections B, C, and D. At a particular cross-section, these vortices are stronger near the top and bottom walls and weaker near the side walls, however, the strength increases with increase in flow rate.
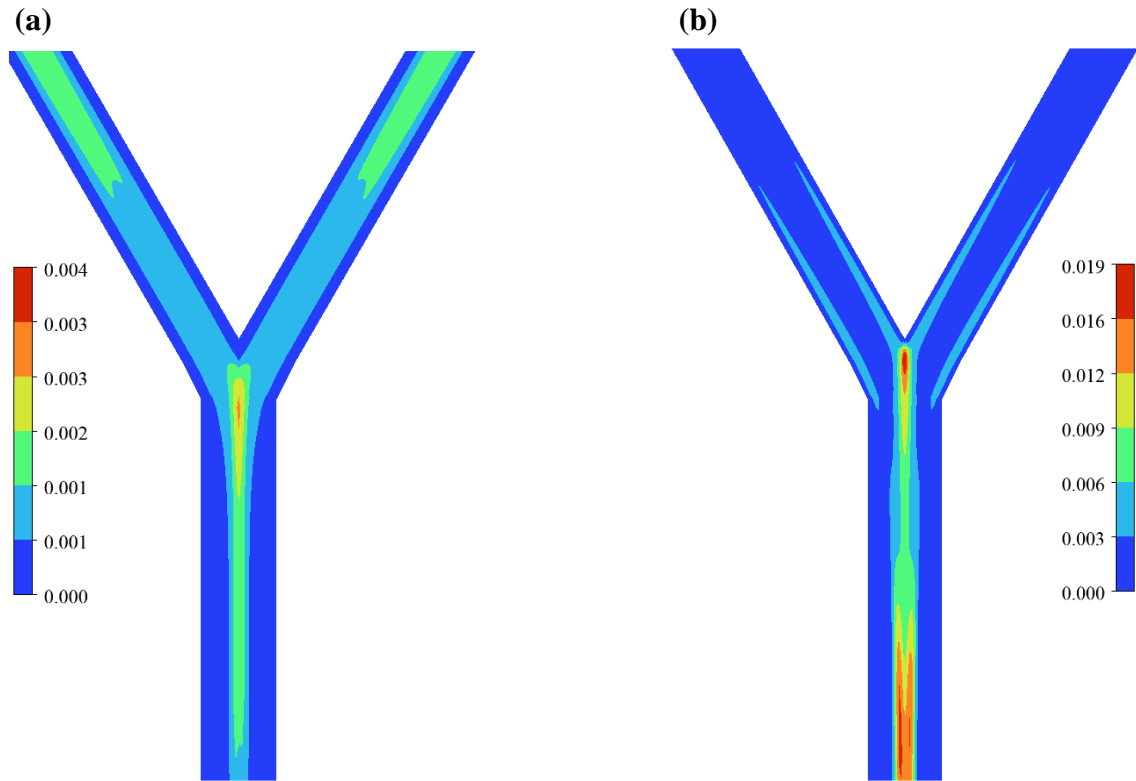
Figure 3. 1: Contours of turbulent kinetic energy (TKE) normalized with respect to inlet velocities against the inlet Reynolds numbers of, (a): 332, (b): 1327. Corresponding tracheal flow rates are 15 l/m and 60 l/m.

Figure 3. 2: Airflow patterns in G3-4 subject to inlet Reynolds number of 332 which correspond to the tracheal flow rate of 15 l/m. Velocity contours highlight the magnitudes of velocity field and velocity vectors visualize the vortices generated because of secondary flows.

Figure 3. 3: Airflow patterns in G3-4 subject to inlet Reynolds number of 1327 which corresponds to tracheal flow rate of 60 l/m. Velocity contours highlight the magnitudes of velocity field and velocity vectors visualize the vortices generated because of secondary flows.

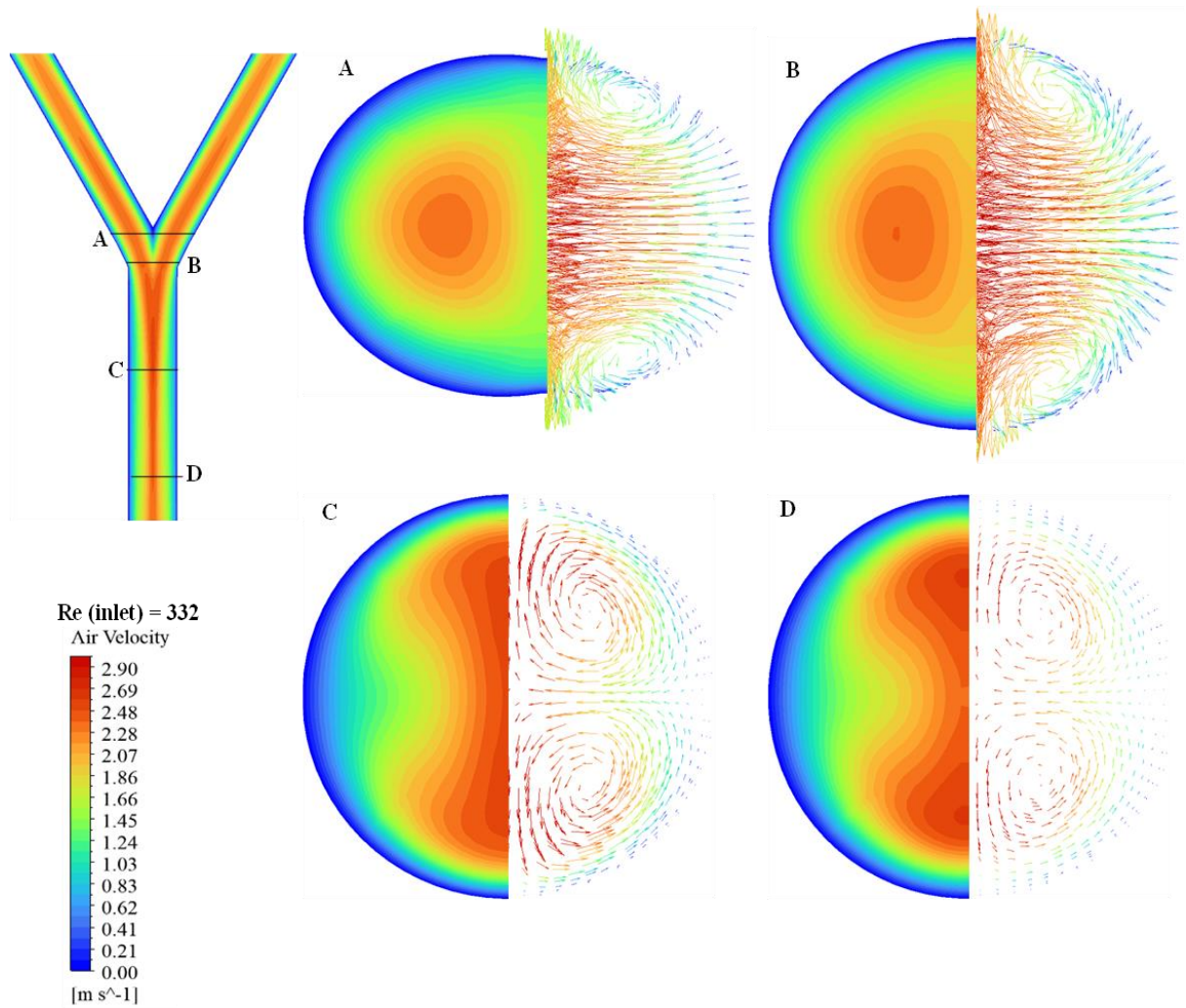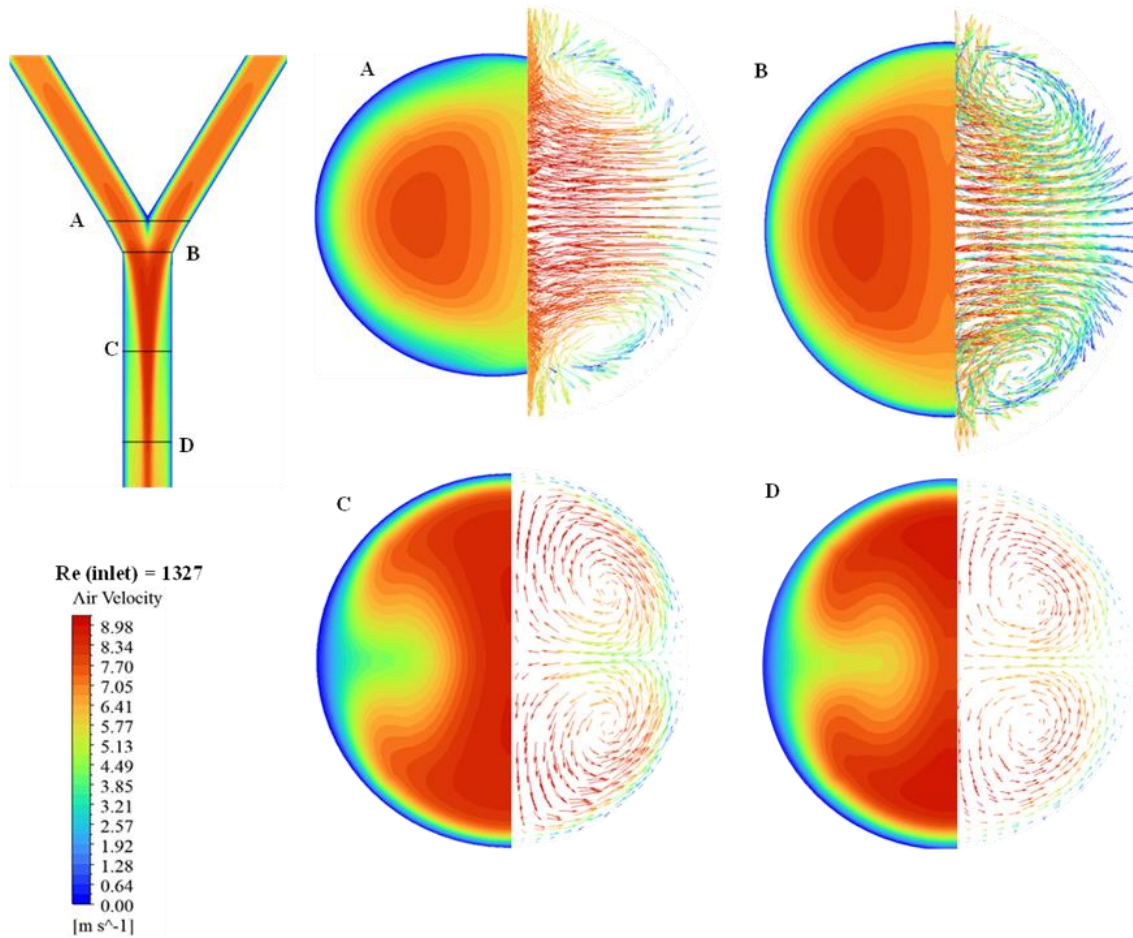*3.1.2 Realistic Lung Model*

In contrast to the idealized lung model, the real lung model exhibits the development of secondary flows in G4 even before reaching the bend at the bifurcation, as evident from sections A and B in Figure 3.4. This early emergence of secondary flows can be attributed to the anatomical complexities present in real airways, such as irregularities in lung geometry, branching angles, and variations in airway diameter along the flow path.

These anatomical features introduce disturbances to the airflow, prompting the formation of secondary flows. In contrast, the absence of such variations in geometric parameters in the idealized lung model results in the absence of secondary flows in G4.
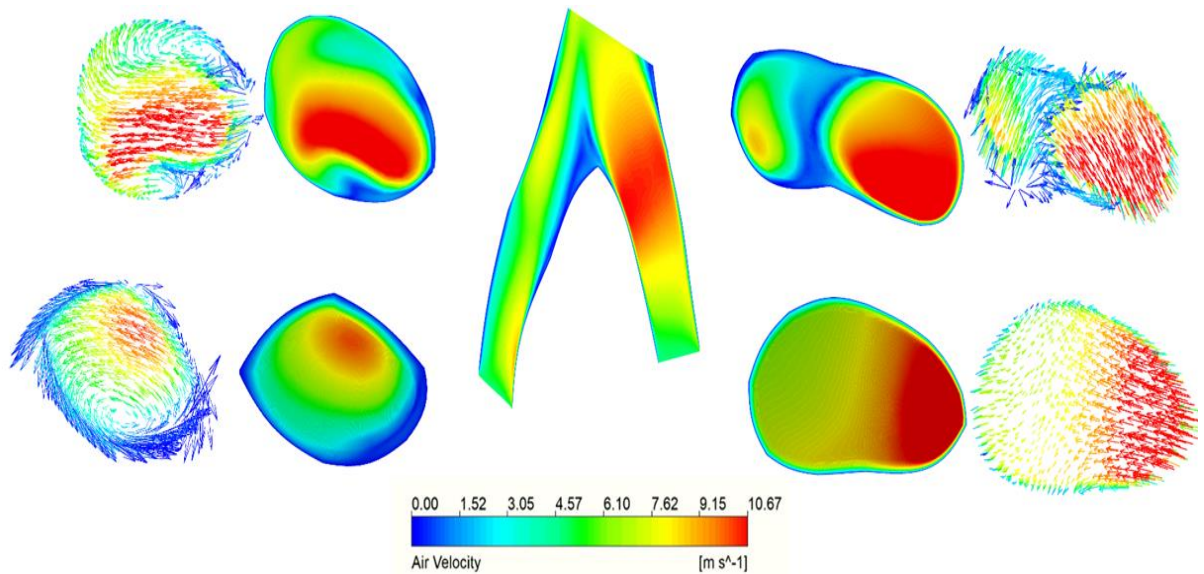
Figure 3. 4: Airflow patterns in the idealized G3-G4 model with inlet Reynolds number of 1327, equivalent to a tracheal flow rate of 60 l/m. Velocity contours show velocity field magnitudes, whereas velocity vectors depict secondary flow structures. Sections A and B depict upstream flows in G4, located away from the cranial ridge. Section C depicts flow slightly downstream of the cranial ridge, while section D shows flow through the plane of G3's output.

3.2 Particle Deposition Analysis

Firstly, deposition patterns between KIM's experimental ideal lung model and the simulated real lung model are compared. Pre- and post-bifurcation zones in the present real lung model correspond to zones 'C' and 'D' respectively in KIM's paper. In contrast to KIM's ideal model, the real lung simulations reveal a notable divergence. KIM noticed deposition primarily in the pre-bifurcation zone. Contrary to KIM's findings, the real lung model simulations reveal deposition principally occurring in the post-bifurcation zone instead of the pre-bifurcation zone (Figure 3.5, 3.6). This unexpected outcome persists across various tracheal flow rates, with deposition varying to some extent with the increase in flow rate (e.g., 90.5% and 9.5% at Q=15lpm, 86.7% and 13.3% at Q=60 lpm for post and pre-bifurcation zones, respectively).

The disparity in deposition patterns between the real and idealized lung models can be attributed to the airflow dynamics illustrated in Figures 3.3and 34. Expiratory deposition is primarily influenced by the presence of secondary flows [22], [20]. In the idealized lung model, G4 is devoid of secondary flows, resulting in minimal deposition within this region, while deposition predominantly occurs in G3, where secondary flows are present. However, in the real lung model, G4 also exhibits secondary flows, leading to particle deposition in this region. Furthermore, the length of G3 in the current segment of G3-G4 is shorter compared to G4, which contributes to less deposition in G3.

The deposition patterns of polydisperse fine and coarse particles (PM2.5, PM10) in relation to workplace pollutants are examined thoroughly using the idealized and real model. Figure 3.7 indicates the patterns of total deposition of polydisperse particles (cumulative deposition of all diameter particles) against different PA intensities in the context of real lung model. Deposition rates of fine particles are comparatively lower than those of coarse particles, primarily due to their lower Stokes numbers. In both cases, a consistent monotonic increase in deposition rates is observed with escalating levels of physical activity.
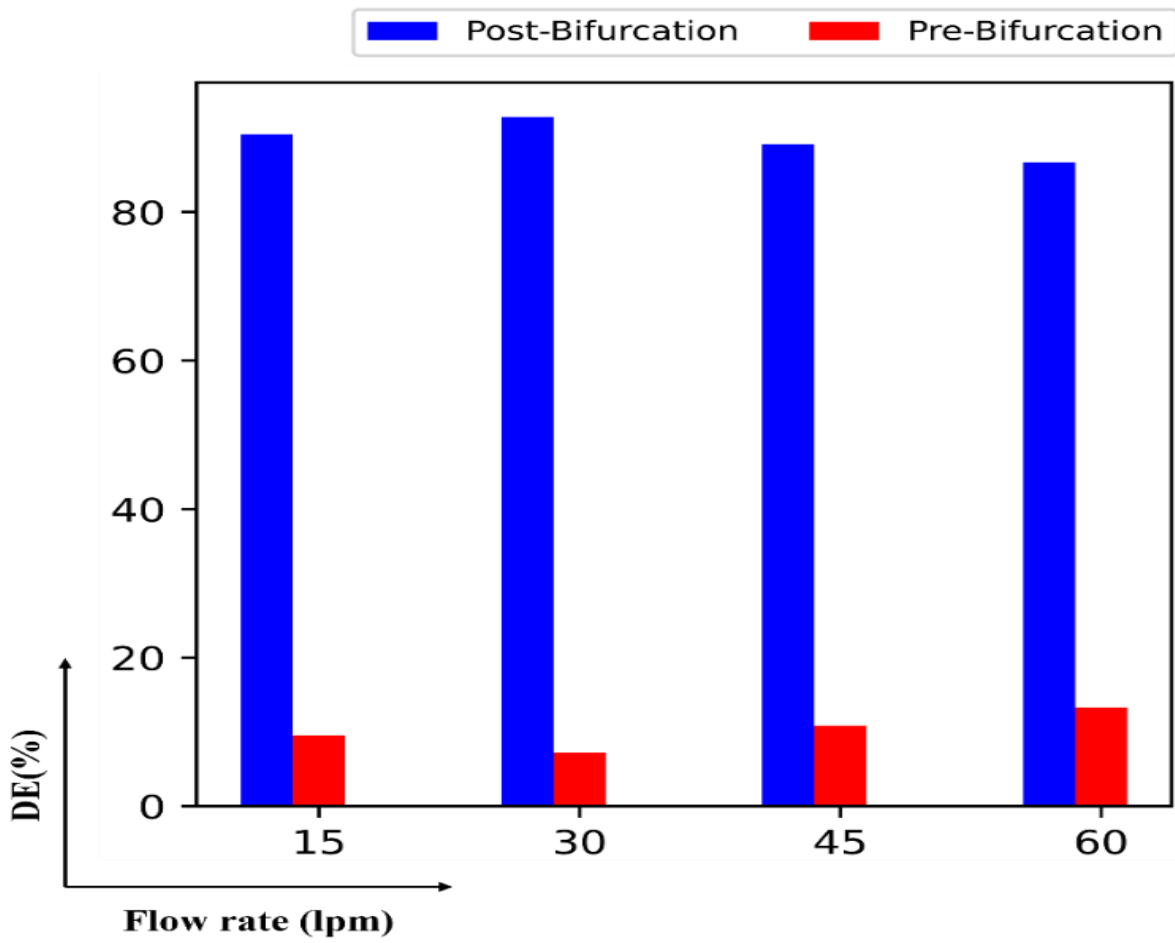
Figure 3. 5: Comparison of % of total deposition at post-bifurcation and pre-bifurcation zones at different levels of tracheal flow rates.

Post-bifurcation (G4)

Pre-bifurcation (G3)

Figure 3. 6: Visualization of deposition patterns. (a): Real lung model, (b): Ideal lung model

Figure 3. 7: Comparative total deposition (DE V/S PA) of polydisperse PM2.5 and PM10 particles for different pollutants - (a) Grain dust, (b) Coal fly ash, (c) Bituminous coal - in the real lung model.

Deposition of polydisperse PM10 particles distribution is also compared to that of two monodisperse distributions of constituent sizes of 5 µm and 10 µm (Figure 3.8) using ideal lung model.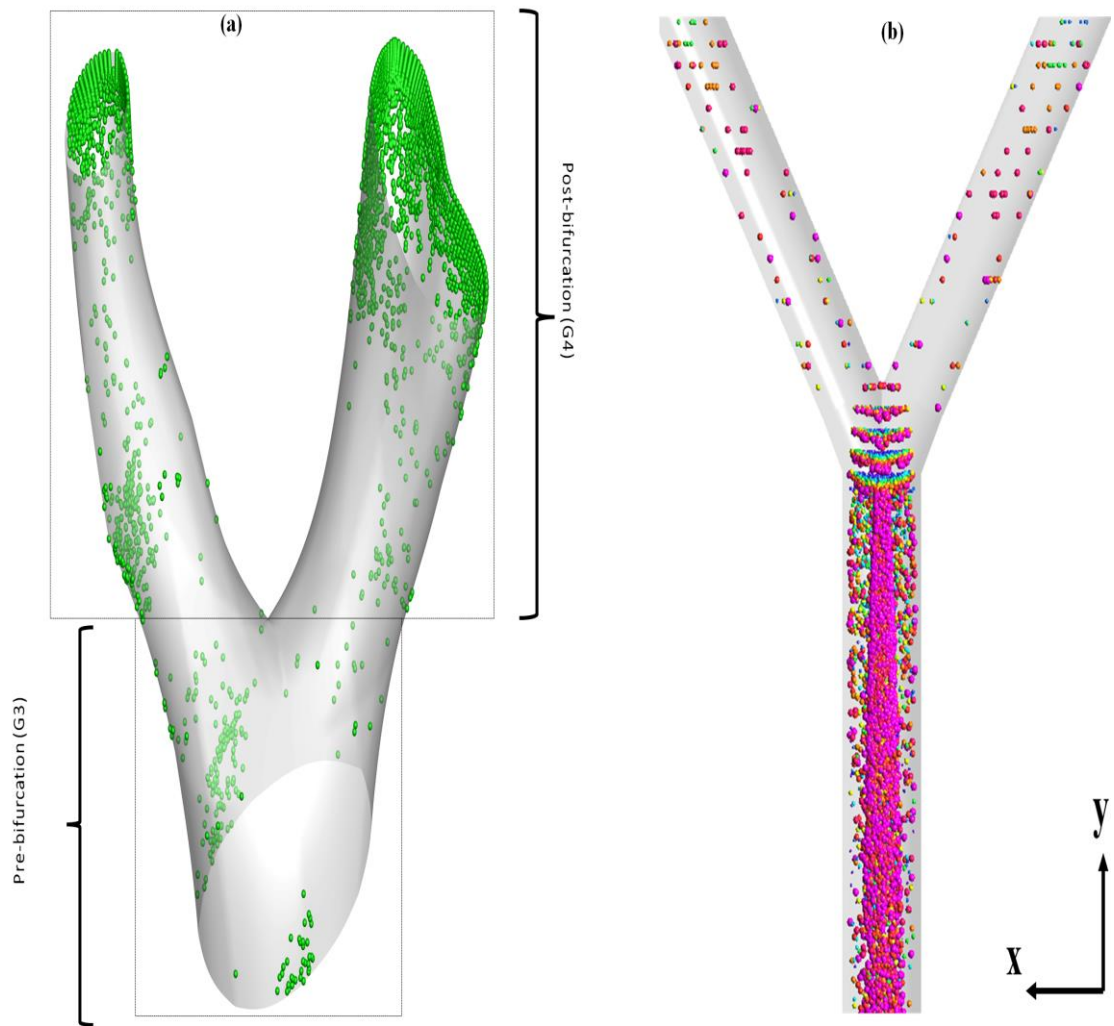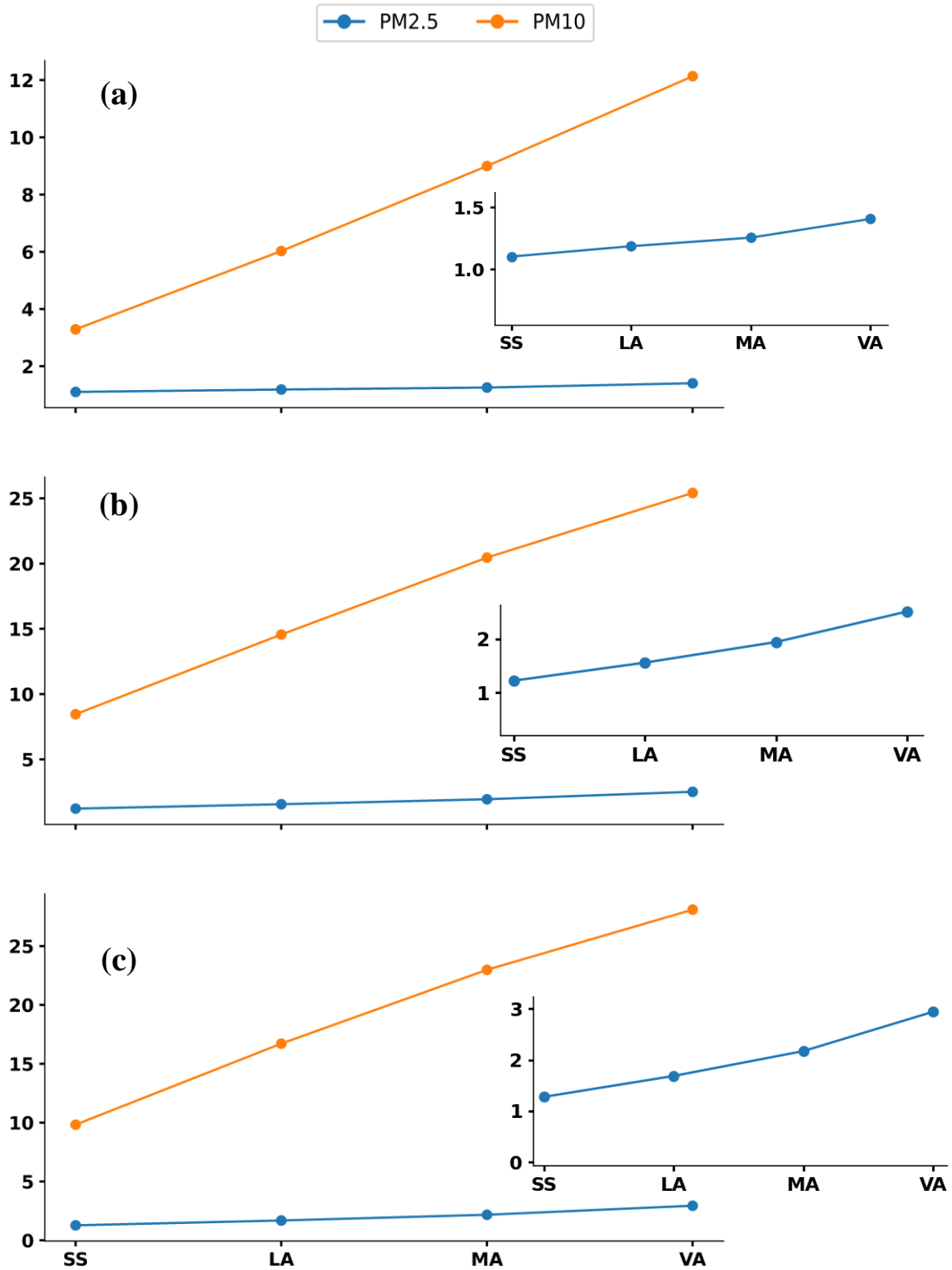 Polydisperse particle deposition is high only for small diameter monodisperse particles. Deposition of large size monodisperse particles exceeds the polydisperse deposition. This analysis attests the hypothesis only for small size monodisperse distribution.
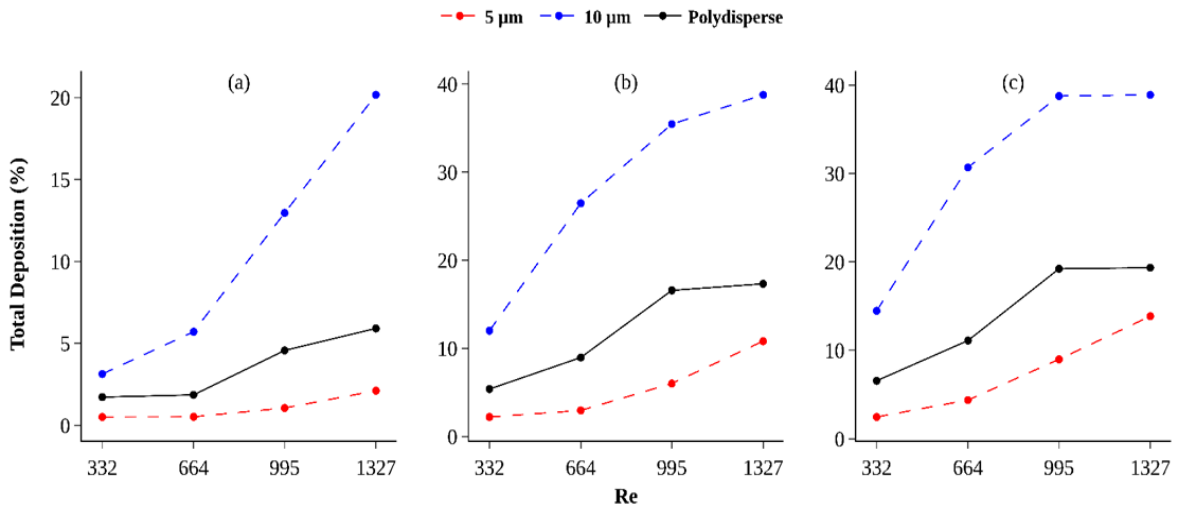

Figure 3. 8: Total deposition comparison of mono and polydisperse particles with reference to inlet Reynolds numbers, (a): GD, (b): CFA, (c): BC

The effect of gravity and secondary flows on deposition rates is evaluated through a comparative analysis utilizing the ideal lung model by including and then excluding the gravity term from the numerical model. The deposition rates of PM10 particles with and without the effects of gravity are shown in Figure 3.9. When gravity was excluded, the DE dropped significantly and small differences in DE were observed at higher flow rates. The analysis indicates that the impact of gravity on deposition is more significant at lower flow rates and less significant at higher flow rates. Deposition in the post-bifurcation zone is governed entirely by gravity only (Figures. 3.10b-13 b).

In ideal lung model, expiratory deposition, in most cases, is observed at the top and bottom walls of parent walls but for higher flow rates and particle densities, it occurs on the side walls also. Convective deposition during exhalation requires the presence of strong secondary vortices and particles reaching the near wall with sufficient inertia to deposit

[22]. At lower flow rates, flow remains laminar and secondary vortices are weak near the side walls, so particles do not deposit on the side walls irrespective of particle density and diameter (Figures 3.10, 3.12 side views). While at higher flow rates, transitional flow generated at the center of airway disperses the particles towards the airway walls and secondary-flow vortices become strong near the side walls. High density particles achieve enough inertia to deposit on the side walls driven by secondary-flow vortices (Figure 3.12 side view). However lower density particles do not reach on side walls even at high flow rates because of low inertia (Figure 3.11 side view).
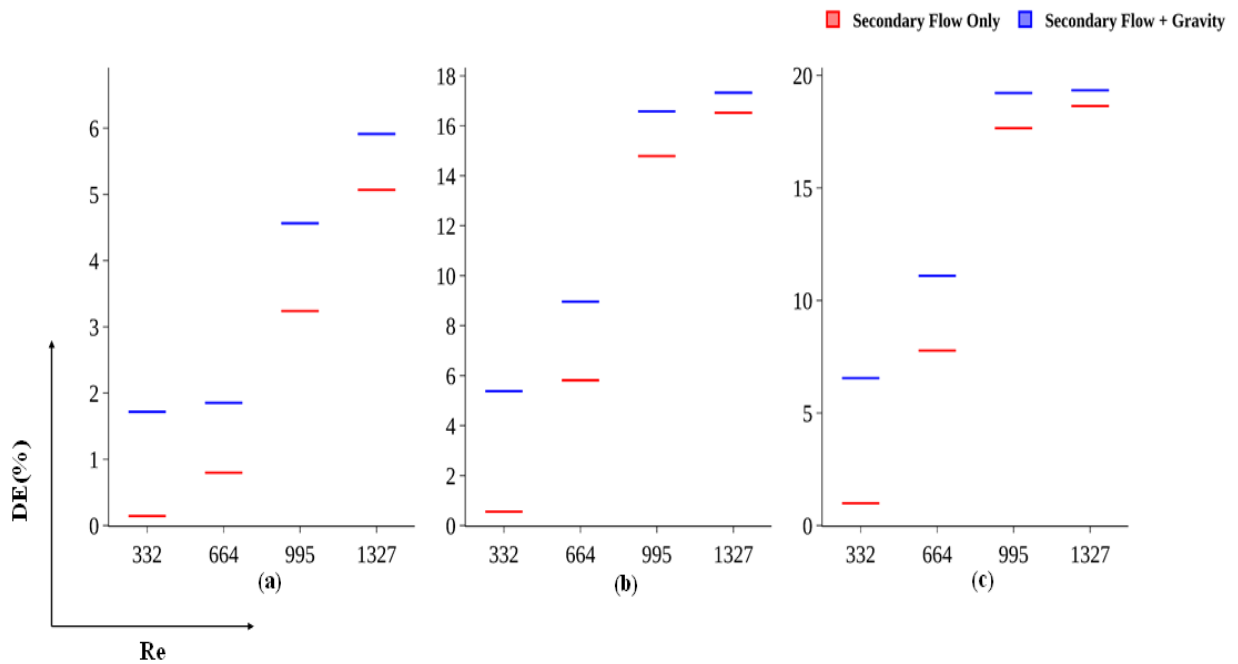
Figure 3. 9: Comparative analysis of impact of gravity on the deposition efficiency of polydisperse PM10 particles. Values along horizontal axis are the Reynolds numbers at G4 inlet. (a) GD, (b) CFA, (c) BC
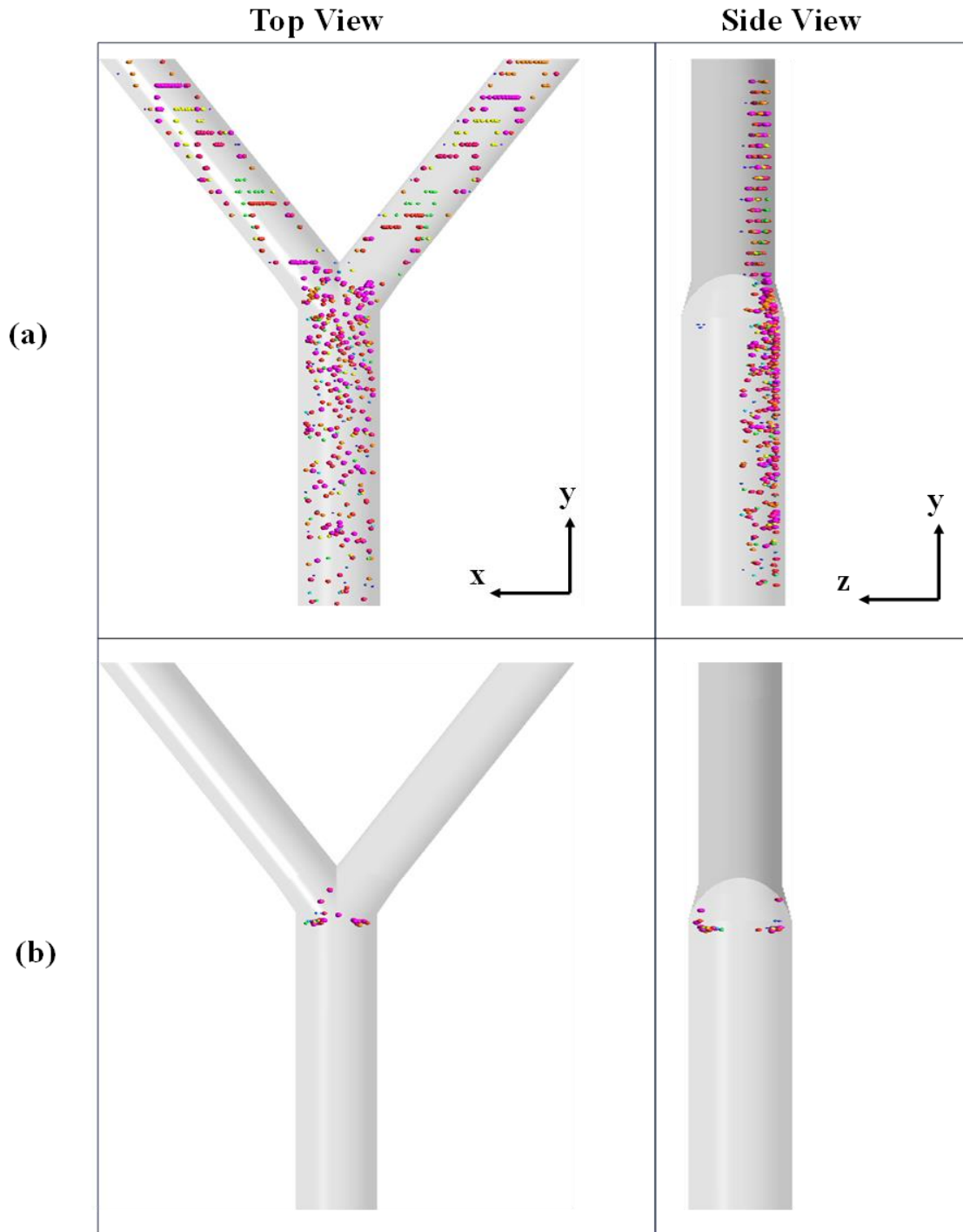
Figure 3. 10: Deposition patterns of polydisperse PM10 particles of GD at inlet Reynolds number 332. (a) represents the combined effect of gravity and secondary flows on deposition. (b) represents the deposition due to secondary flows only.

Top View   **Side View**

(a)

(b)
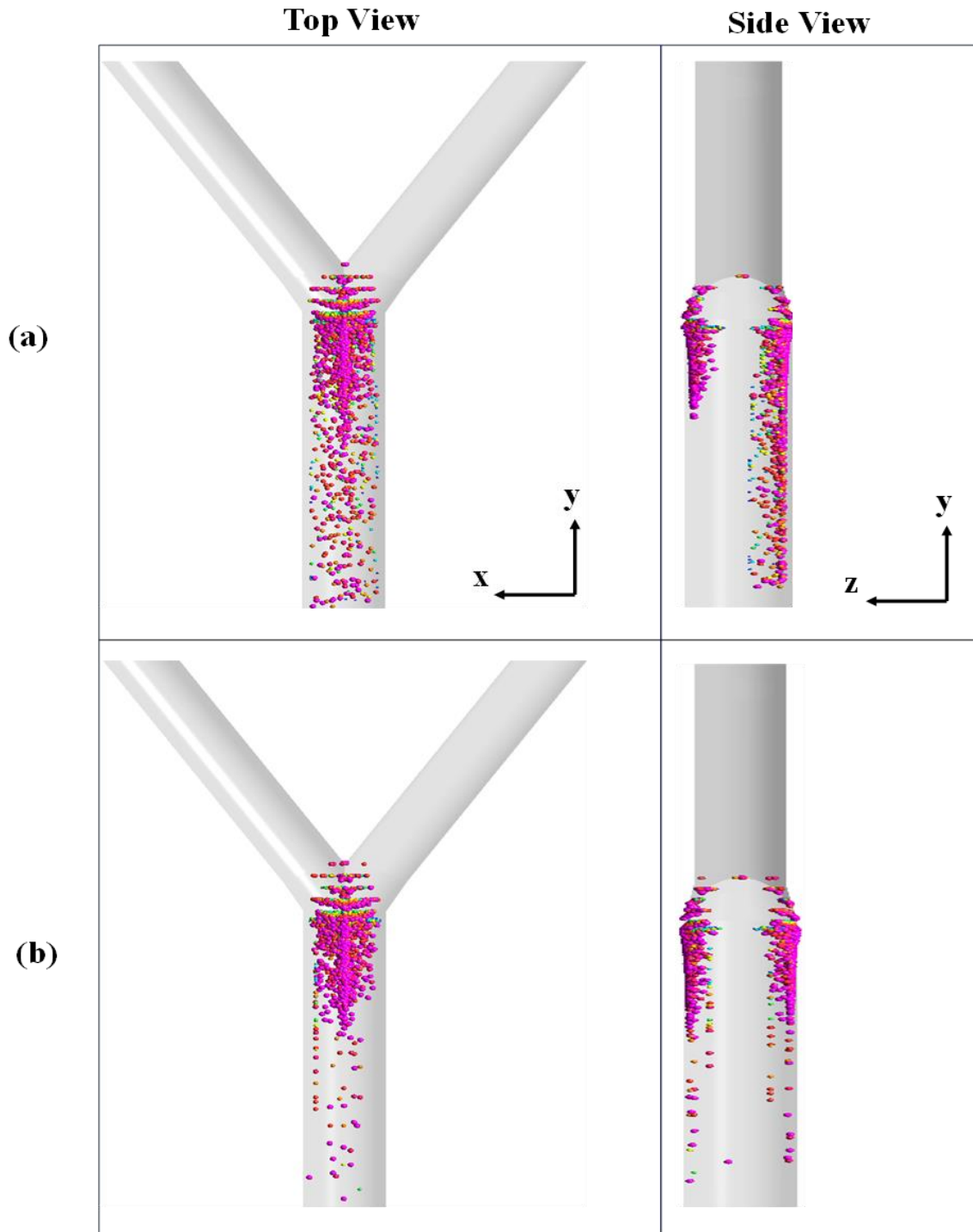
Re = 1327

Figure 3. 11: Deposition patterns of polydisperse PM10 particles of GD at inlet Reynolds number 1327. (a) represents the combined effect of gravity and secondary flows on deposition. (b) represents the deposition due to secondary flows only.

Figure 3. 12: Deposition patterns of polydisperse PM10 particles of BC at inlet Reynolds number 332. (a) represents the combined effect of gravity and secondary flows on deposition. (b) represents the deposition due to secondary flows only.

Top View   **Side View**

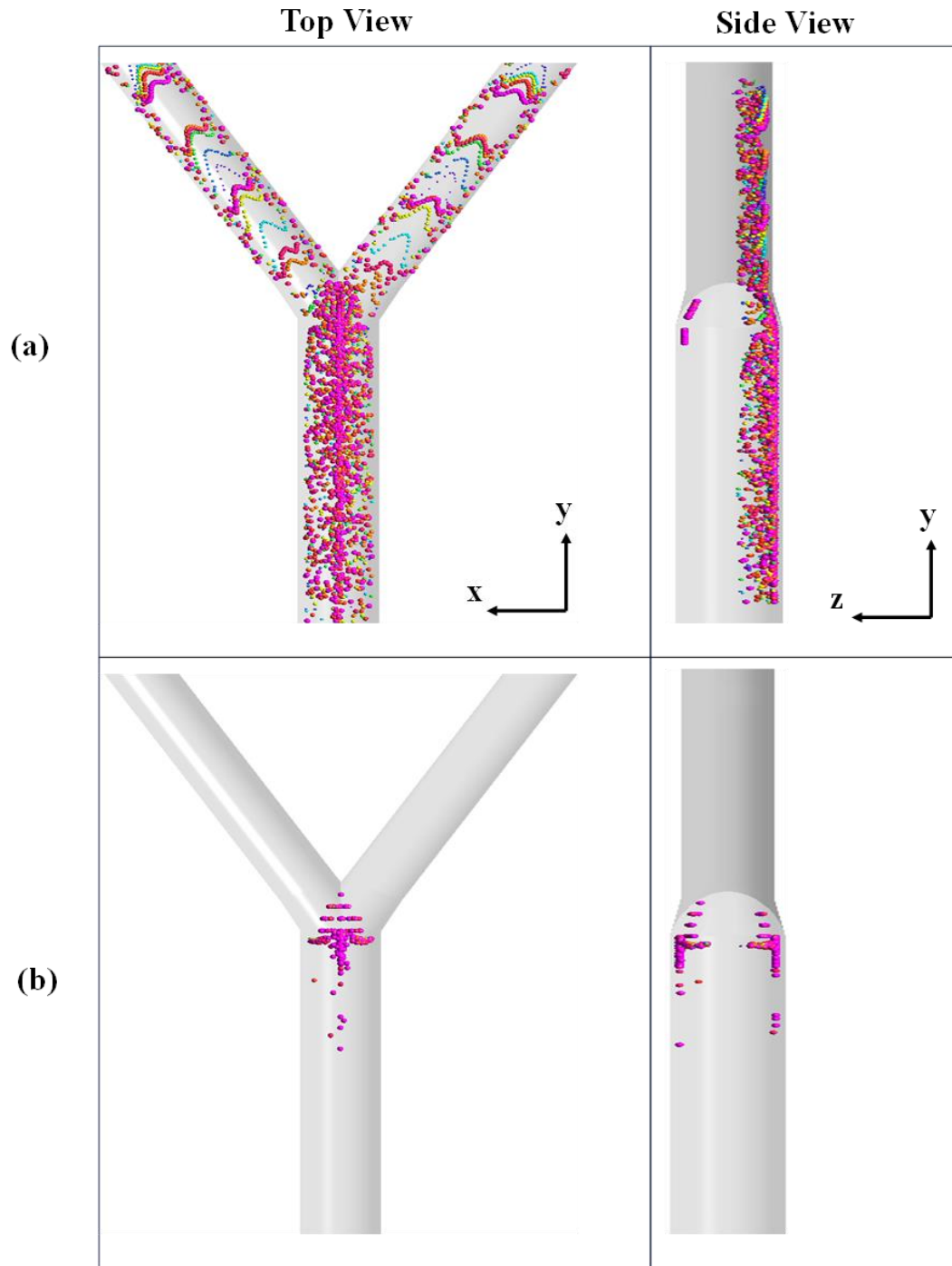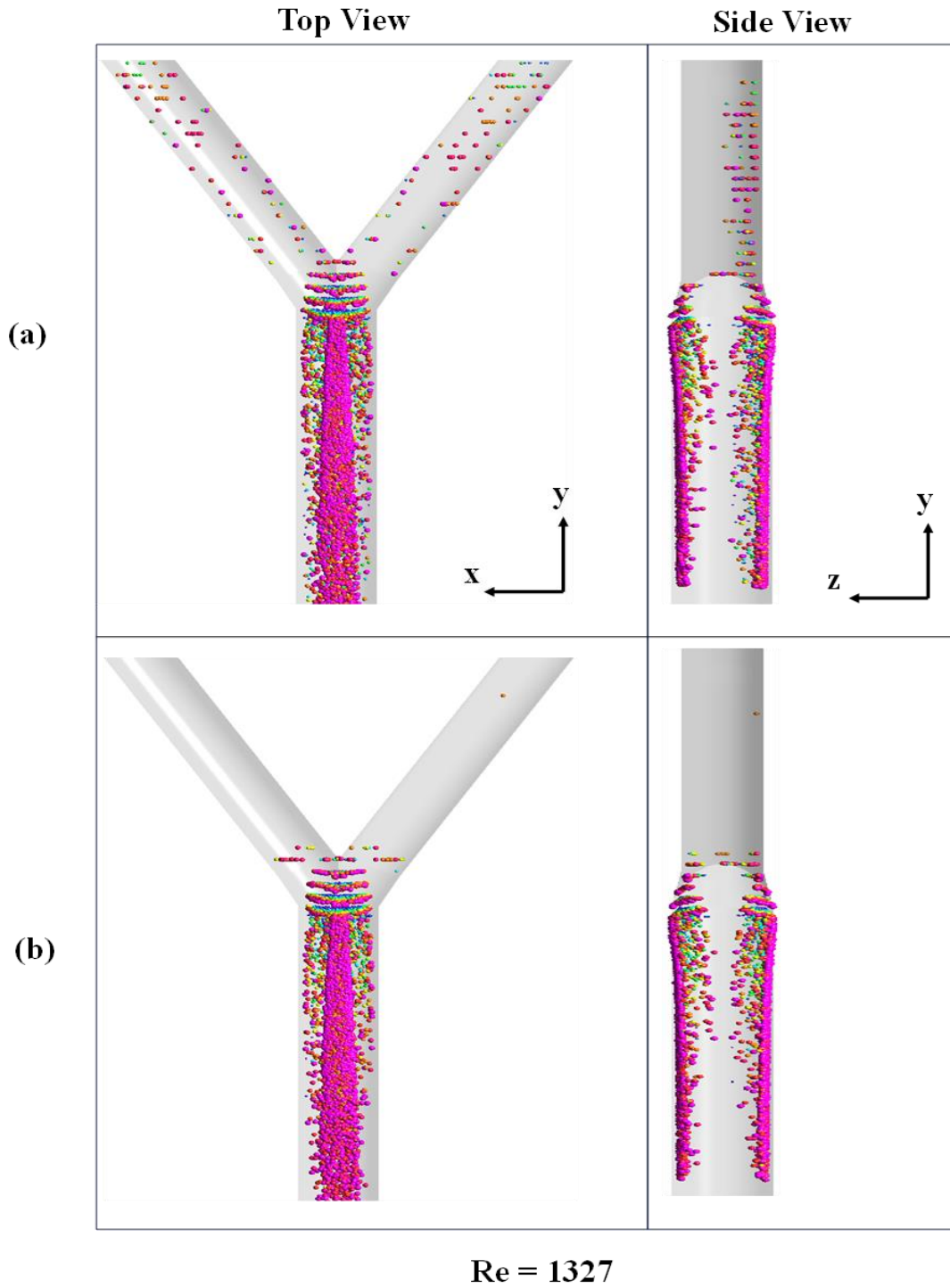**(a)**

(b)

Re = 1327

Figure 3. 13: Deposition patterns of polydisperse PM10 particles of BC at inlet Reynolds number 1327. (a) represents the combined effect of gravity and secondary flows on deposition. (b) represents the deposition due to secondary flows only.

A comparison of inspiratory and expiratory depositions is performed on PM10 coal particles. Due to inertial impaction, inspiratory deposition remains higher than expiratory deposition (Figure 3.14).
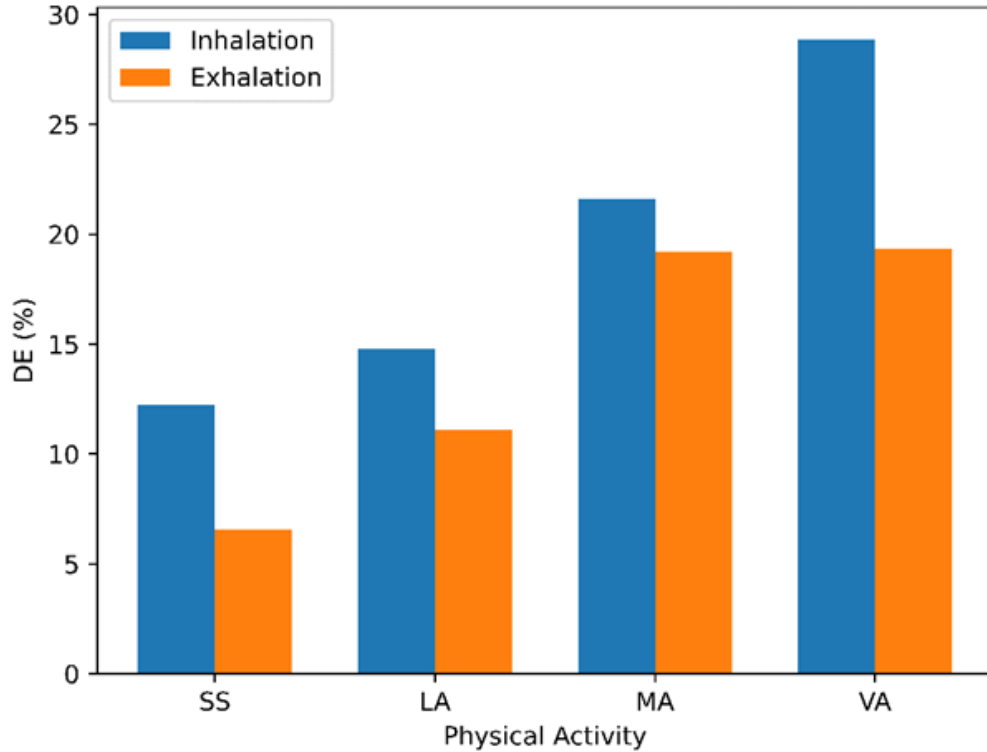
Figure 3. 14: Comparison of inspiratory and expiratory deposition rates in G3-G4

Figures 3.15-18 illustrate the deposition patterns of individual PM2.5 and PM10 particle diameters in polydisperse injection for real and ideal lung geometries, respectively. In the ideal lung model, PM2.5 deposition is notably low, with the highest efficiency observed for 2.05 µm at 1.87%. The relationship between deposition efficiency and particle diameter appears random. Conversely, in the real lung model, PM2.5 deposition is more substantial, with only 1.15 µm particles exhibiting less than 1% efficiency. Grain dust particles in PM2.5 display some level of randomness in deposition efficiency. For PM10 particles, deposition efficiency rises with particle diameter and physical activity intensity, observed across both ideal and real lung models.

Figure 3. 15: Deposition of PM2.5 individual particle diameters based on their initial distributions (Ideal lung model).
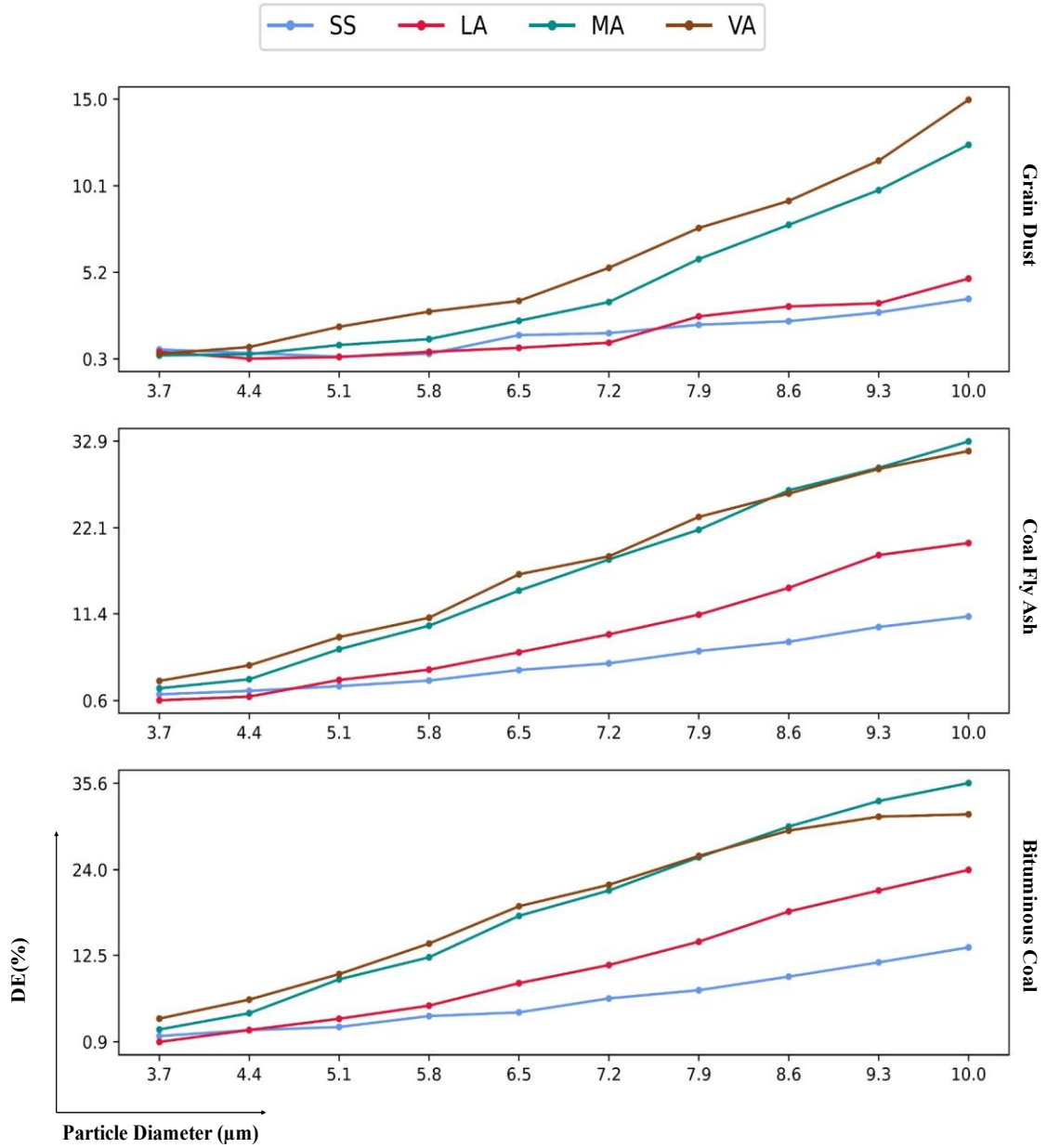
Figure 3. 16: Deposition of PM10 individual particle diameters based on their initial distributions (Ideal lung model).

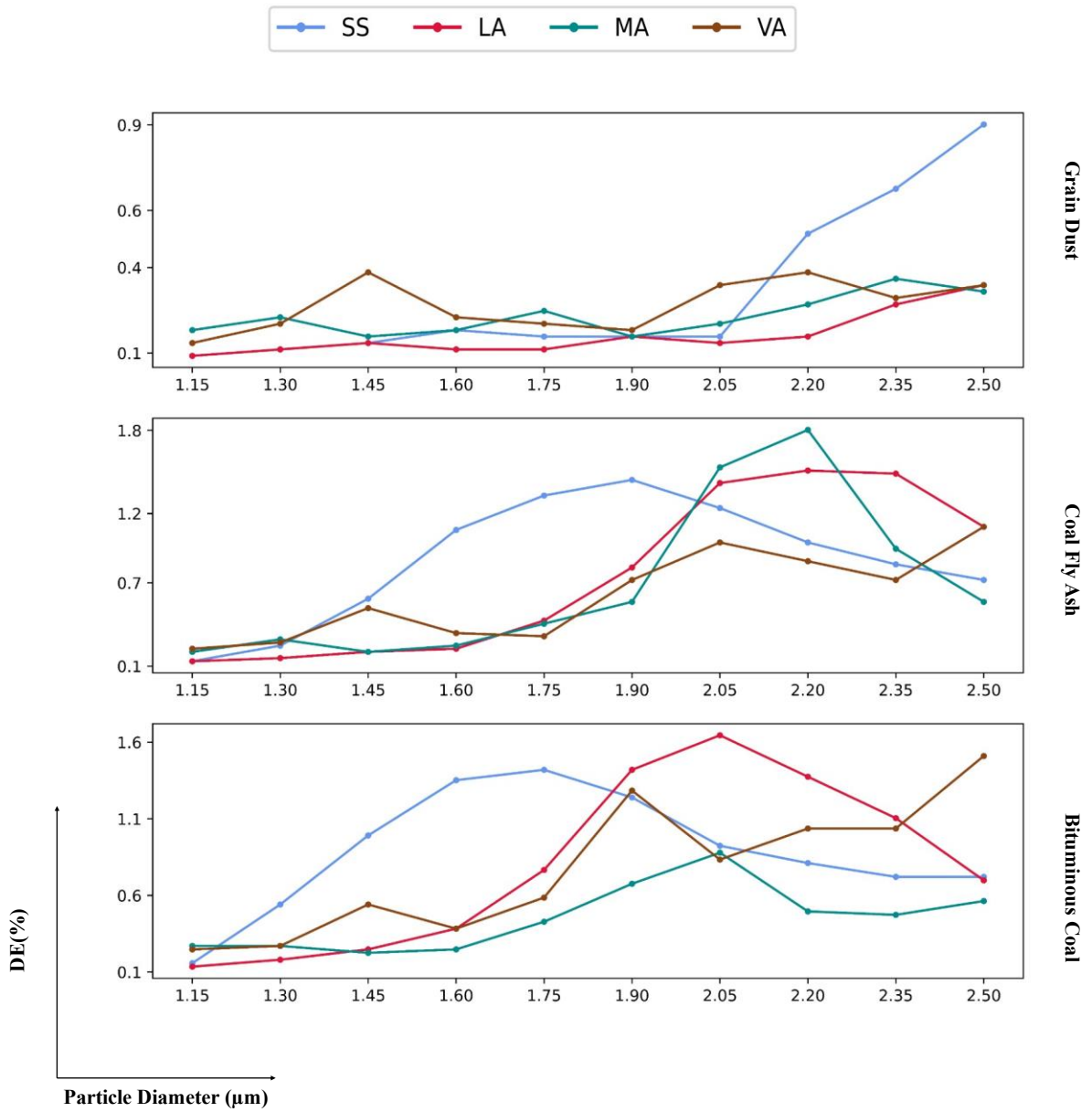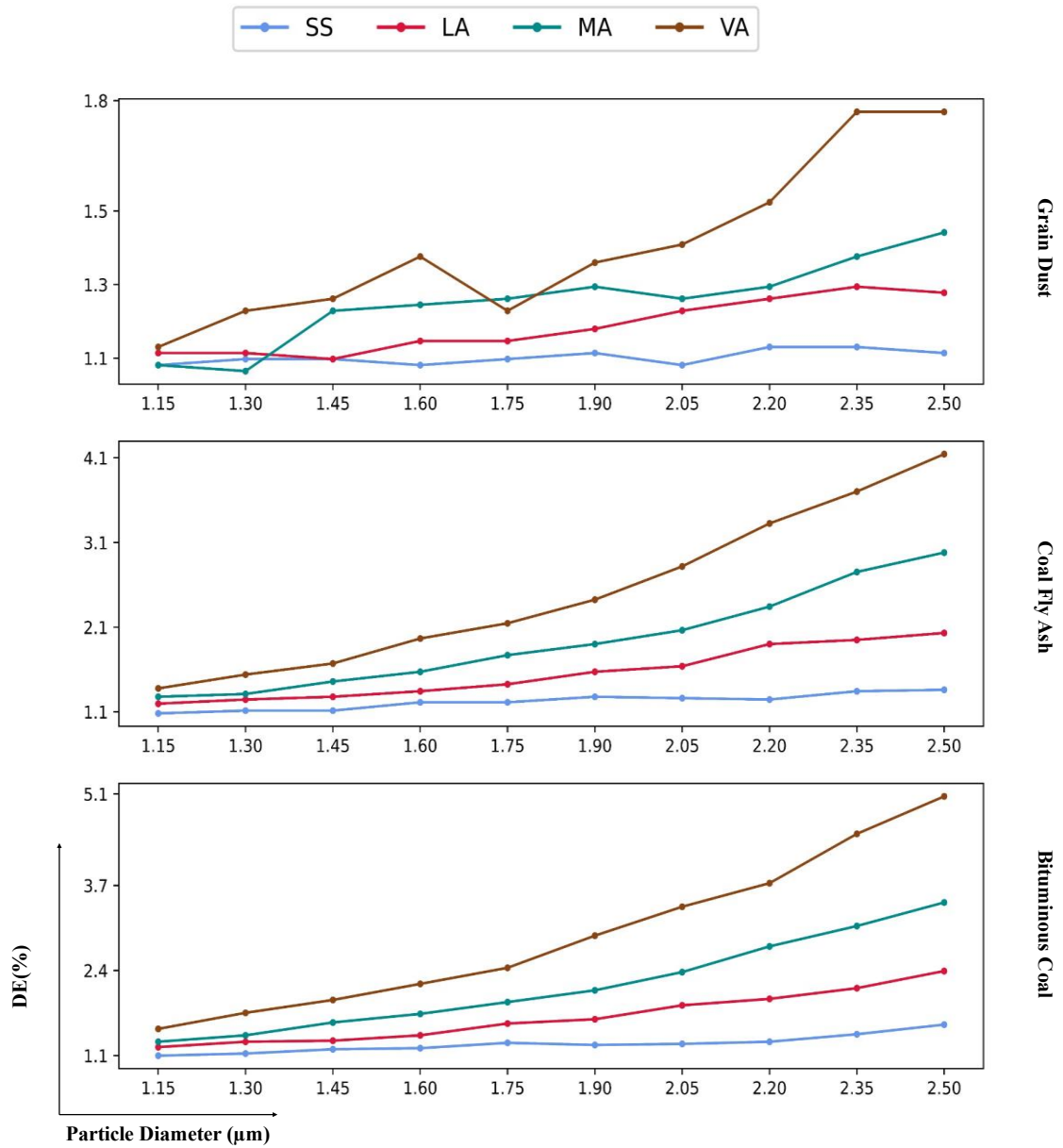**Figure 3. 17:** Deposition of PM2.5 individual particle diameters based on their initial distributions (Real lung model).
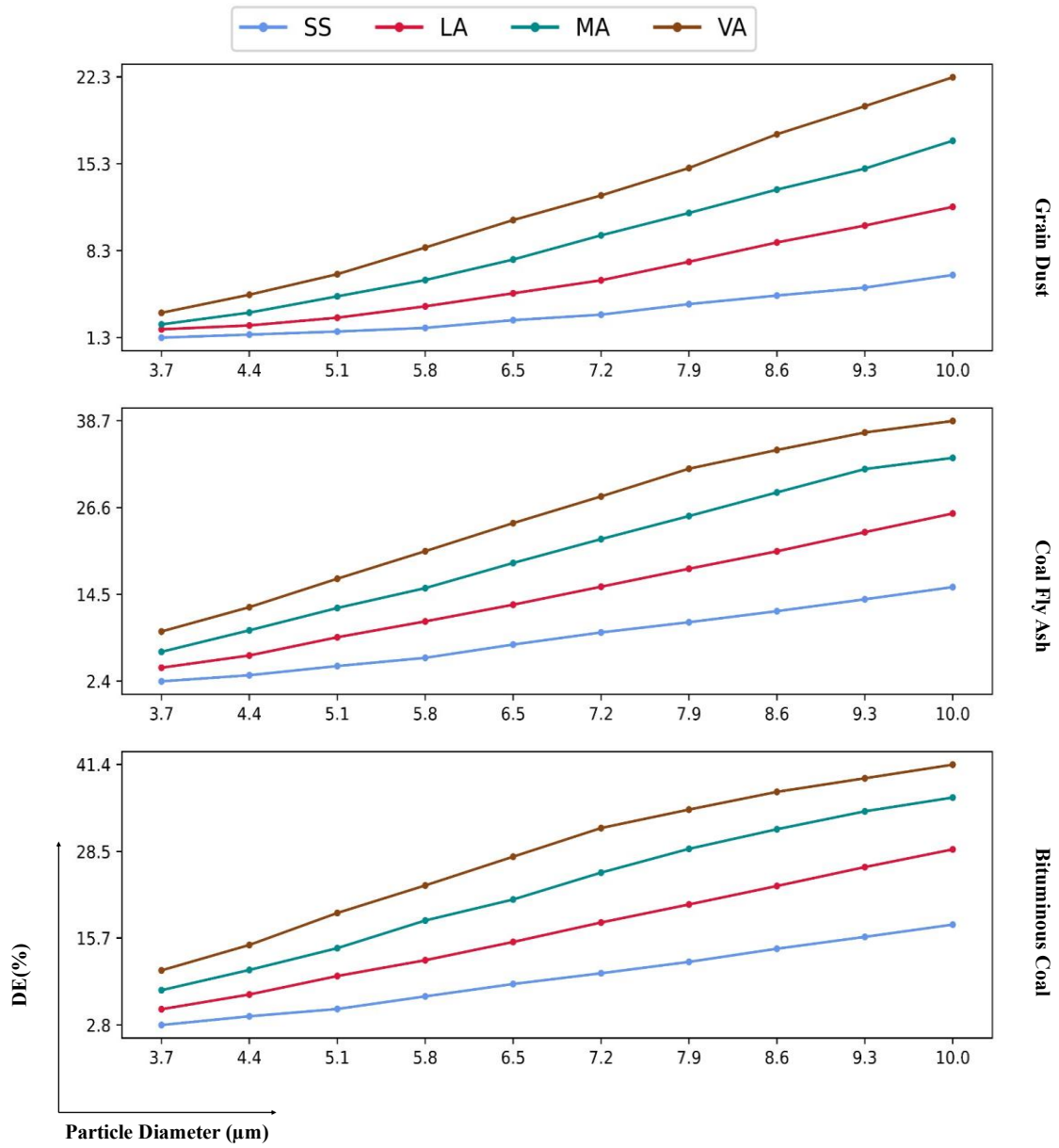
Figure 3. 18: Deposition of PM10 individual particle diameters based on their initial distributions (Real lung model).

Figures 3.19, 3.20 offer a detailed examination of workplace pollutant deposition at different physical activity levels, considering a real lung model in idealized and real lung geometries respectively. The findings indicate that individuals involved in high-intensity activities, such as those in grain processing, coal mines, and fly ash brick industries, are prone to increased pollutant particle deposition. This heightened exposure in occupational settings raises concerns about potential risks of lung-related diseases.
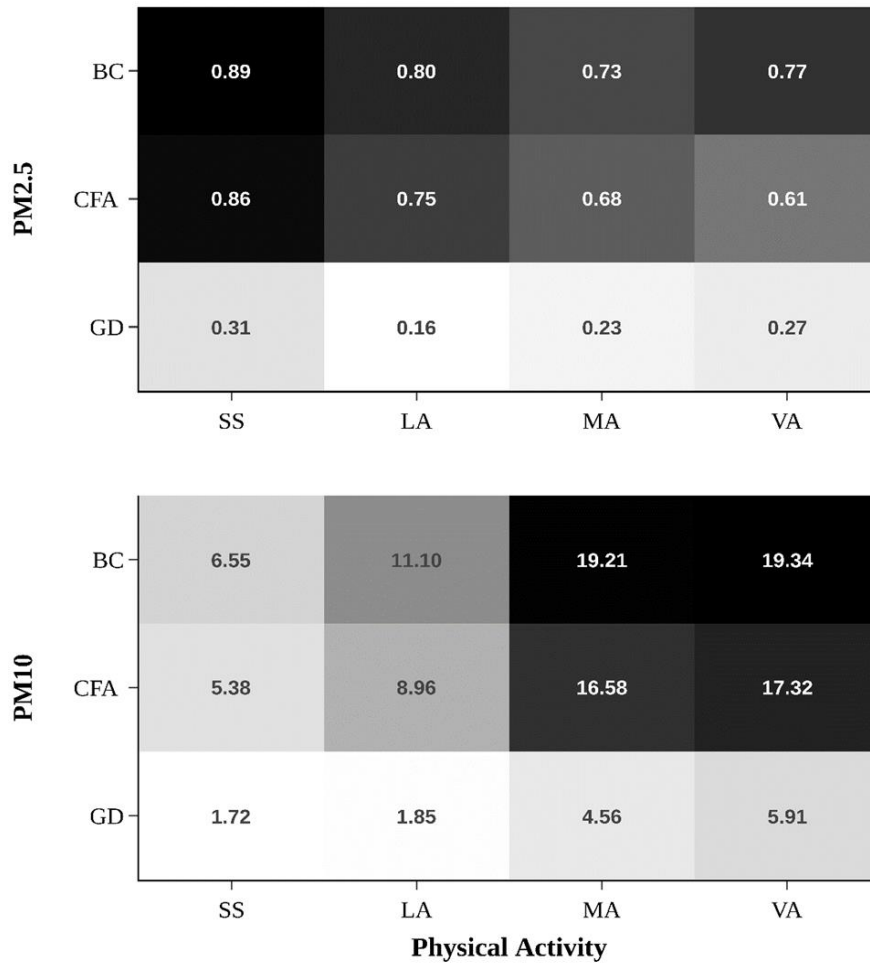
Figure 3. 19: Deposition efficiency trends of PM2.5 and PM10 particles in relation to physical activity intensity and pollutant type (Ideal geometry).
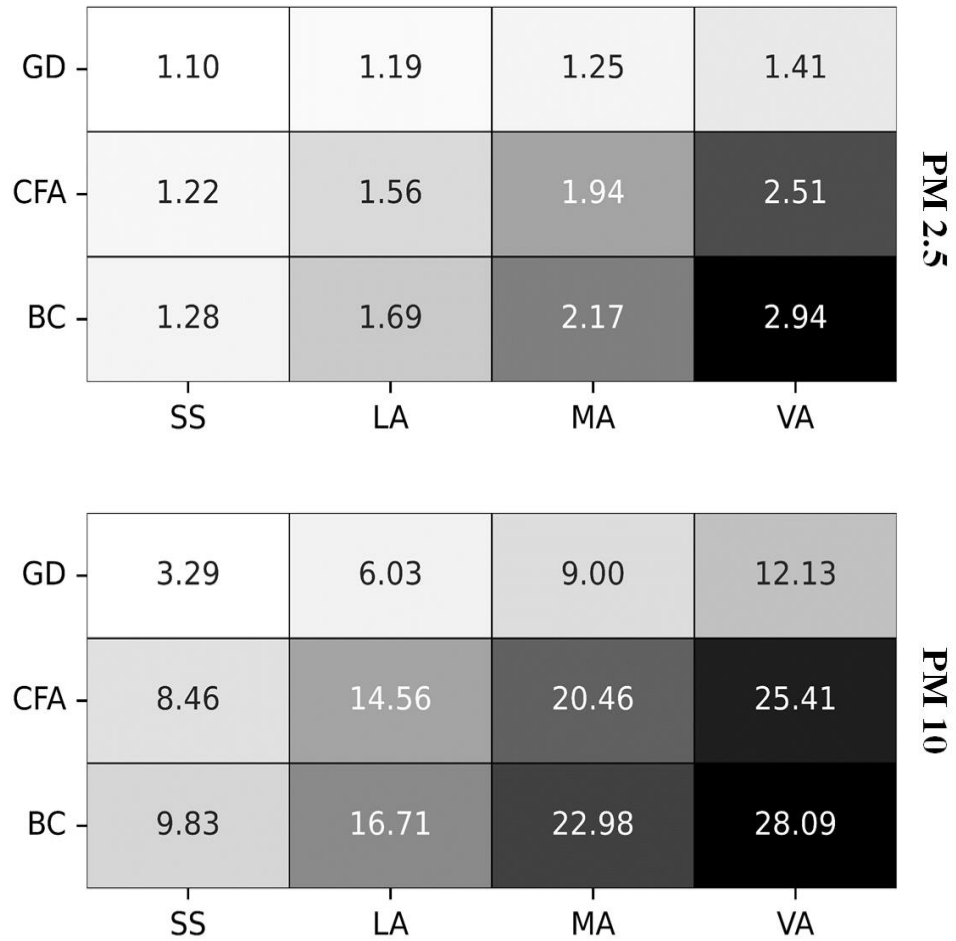
Figure 3. 20: Deposition efficiency trends of PM2.5 and PM10 particles in relation to physical activity intensity and pollutant type (Real geometry).

CHAPTER 4: CONCLUSIONS AND FUTURE RECOMMENDATION

A numerical study is performed on idealized and real models of airways G3-G4 to investigate the deposition patterns of fine (PM2.5) and coarse (PM10) polydisperse particles specifically during exhalation. The effects of varying levels of physical activity on the deposition of pollutant particles of grain dust, coal fly ash, and bituminous coal are studied. Deposition trends of mono and polydisperse particles are also compared.

4.1 Conclusion

Key findings from the study include:

• In the real airway model, anatomical complexities lead to an early emergence of secondary flows, whereas in the idealized model, these secondary flows occur after the flow passes the cranial ridge.

• A notable shift in deposition patterns from pre- to post-bifurcation zones is observed in the real model compared to the idealized model.

• During inhalation, deposition primarily occurs near the cranial ridge due to inertial impaction, while exhalation results in deposition shifting to the pre- and post-bifurcation zones.

• The effect of gravity on deposition, compared to secondary flow, is more pronounced at lower flow rates but diminishes at higher flow rates.

• PM2.5 deposition is minimal and random in the idealized model but becomes more significant and consistent in the real model. Substantial deposition rates are observed for PM10 particles.

• Deposition of particles of grain dust, fly ash, and coal particles has a direct relation with the intensity of PA.

4.2 Future Work

Although recent studies have made significant progress in explaining inspiratory deposition, there is still a significant knowledge vacuum about expiratory deposition dynamics. This work aims to close this gap by performing an extensive analysis of exhalation-driven deposition procedures. Comprehending the complex interactions between particle behavior during expiration is essential to comprehending all of the deposition patterns in contaminated settings. While we have concentrated on a single bifurcation in the lung model, we want to expand our research in the future to include several generations of the realistic lung model. With this extension, we want to provide a more thorough knowledge of the kinetics of particle deposition throughout the respiratory tract by analyzing a wider variety of airway generations.

Furthermore, although though the focus of this work has been on dry particles, it is important to note that particles turn hygroscopic as soon as they enter the lungs. Therefore, to gain greater understanding of the intricate processes controlling respiratory exposure to airborne contaminants, future study will also examine the impact of hygroscopicity on particle deposition behavior. Our understanding of pollutant exposure processes and how they affect lung health will grow as a result of this iterative approach, opening the door to more potent risk-reduction tactics for the environment.

REFERENCES

[1]   W. H. Organization, "Air pollution." 2023.

[2]   C. Nishida and K. Yatera, "The Impact of Ambient Environmental and Occupational Pollution on Respiratory Diseases," *Int J Environ Res Public Health*, vol. 19, no. 5, Dec. 2022, doi: 10.3390/ijerph19052788.

[3]   R. Paul, O. Adeyemi, and A. A. Arif, "Estimating mortality from coal workers' pneumoconiosis among Medicare beneficiaries with pneumoconiosis using binary regressions for spatially sparse data," *Am J Ind Med*, vol. 65, no. 4, pp. 262–267, Dec. 2022, doi: 10.1002/ajim.23330.

[4]   S. Quirce and A. Diaz-Perales, "Diagnosis and management of grain-induced asthma," *Allergy, Asthma and Immunology Research*, vol. 5, no. 6. pp. 348–356, Dec. 2013. doi: 10.4168/aair.2013.5.6.348.

[5]   O. Vandenplas, "Occupational Asthma: Etiologies and Risk Factors," *Allergy Asthma Immunol Res*, vol. 3, no. 3, p. 157, 2011, doi: 10.4168/aair.2011.3.3.157.

[6]   N. Gupta, V. V Gedam, C. Moghe, and P. Labhasetwar, "Investigation of characteristics and leaching behavior of coal fly ash, coal fly ash bricks and clay bricks," *Environ Technol Innov*, vol. 7, pp. 152–159, 2017, doi: https://doi.org/10.1016/j.eti.2017.02.002.

[7]   K. M. Zierold and C. Odoh, "A review on fly ash from coal-fired power plants: chemical composition, regulations, and health evidence," *Rev Environ Health*, vol. 35, no. 4, pp. 401–418, Dec. 2020, doi: 10.1515/reveh-2019-0039.

[8]   S. Gautam, A. K. Patra, S. P. Sahu, and M. Hitch, "Particulate matter pollution in opencast coal mining areas: a threat to human health and environment," *Int J Min Reclam Environ*, vol. 32, no. 2, pp. 75–92, Dec. 2018, doi: 10.1080/17480930.2016.1218110.

[9]   K. Iyogun, S. A. Lateef, and G. R. E. E. Ana, "Lung Function of Grain Millers Exposed to Grain Dust and Diesel Exhaust in Two Food Markets in Ibadan Metropolis, Nigeria," *Saf Health Work*, vol. 10, no. 1, pp. 47–53, 2019, doi: https://doi.org/10.1016/j.shaw.2018.01.002.

[10]   L. G. V. Buonfiglio *et al.*, "Effects of Coal Fly Ash Particulate Matter on the Antimicrobial Activity of Airway Surface Liquid," *Environ Health Perspect*, vol. 125, no. 7, Dec. 2017, doi: 10.1289/EHP876.

[11]   G. Morantes, J. C. González, and G. Rincón, "Characterisation of particulate matter and identification of emission sources in Greater Caracas, Venezuela," *Air Qual*

Atmos Health, vol. 14, no. 12, pp. 1989–2014, 2021, doi: 10.1007/s11869-021-01070-2.

[12]   W. Hofmann, "Modelling inhaled particle deposition in the human lung—A review," *J Aerosol Sci*, vol. 42, no. 10, pp. 693–724, 2011, doi: https://doi.org/10.1016/j.jaerosci.2011.05.007.

[13]   P. W. Longest, S. Vinchurkar, and T. Martonen, "Transport and deposition of respiratory aerosols in models of childhood asthma," *J Aerosol Sci*, vol. 37, no. 10, pp. 1234–1257, 2006, doi: https://doi.org/10.1016/j.jaerosci.2006.01.011.

[14]   N. A. H. Janssen, P. Fischer, M. Marra, C. Ameling, and F. R. Cassee, "Short-term effects of PM2.5, PM10 and PM2.5–10 on daily mortality in the Netherlands," *Science of The Total Environment*, vol. 463–464, pp. 20–26, 2013, doi: https://doi.org/10.1016/j.scitotenv.2013.05.062.

[15]   F. Lu *et al.*, "Systematic review and meta-analysis of the adverse health effects of ambient PM2.5 and PM10 pollution in the Chinese population," *Environ Res*, vol. 136, pp. 196–204, 2015, doi: https://doi.org/10.1016/j.envres.2014.06.029.

[16]   O. Hahad *et al.*, "Physical Activity in Polluted Air—Net Benefit or Harm to Cardiovascular Health? A Comprehensive Review," *Antioxidants*, vol. 10, no. 11, p. 1787, Dec. 2021, doi: 10.3390/antiox10111787.

[17]   O. Hahad, A. Daiber, and T. Münzel, "Physical activity in polluted air: an urgent call to study the health risks," *Lancet Planet Health*, vol. 7, no. 4, pp. e266–e267, Dec. 2023, doi: 10.1016/S2542-5196(23)00055-4.

[18]   E. M. Saber and G. Heydari, "Flow patterns and deposition fraction of particles in the range of 0.1–10μm at trachea and the first third generations under different breathing conditions," *Comput Biol Med*, vol. 42, no. 5, pp. 631–638, Dec. 2012, doi: 10.1016/j.compbiomed.2012.03.002.

[19]   Q. Deng, C. Ou, Y.-M. Shen, Y. Xiang, Y. Miao, and Y. Li, "Health effects of physical activity as predicted by particle deposition in the human respiratory tract," *Science of The Total Environment*, vol. 657, pp. 819–826, Dec. 2019, doi: 10.1016/j.scitotenv.2018.12.067.

[20]   C. S. KIM, A. J. IGLESIAS, and L. GARCIA, "Deposition of Inhaled Particles in Bifurcating Airway Models: II. Expiratory Deposition," *Journal of Aerosol Medicine*, vol. 2, no. 1, pp. 15–27, Dec. 1989, doi: 10.1089/jam.1989.2.15.

[21]   I. Balásházy and W. Hofmann, "Particle deposition in airway bifurcations–II. Expiratory flow," *J Aerosol Sci*, vol. 24, no. 6, pp. 773–786, 1993, doi: https://doi.org/10.1016/0021-8502(93)90045-B.

[22] P. W. Longest and S. Vinchurkar, "Inertial deposition of aerosols in bifurcating models during steady expiratory flow," *J Aerosol Sci*, vol. 40, no. 4, pp. 370–378, 2009, doi: https://doi.org/10.1016/j.jaerosci.2008.11.007.

[23] M. S. Islam, S. C. Saha[1], E. Sauret, Y. T. Gu, and Z. D. Ristovski, "Numerical Investigation of Aerosol Particle Transport and Deposition in Realistic Lung Airway."

[24] M. Rahimi-Gorji, O. Pourmehran, M. Gorji-Bandpy, and T. B. Gorji, "CFD simulation of airflow behavior and particle transport and deposition in different breathing conditions through the realistic model of human airways," *J Mol Liq*, vol. 209, pp. 121–133, Sep. 2015, doi: 10.1016/j.molliq.2015.05.031.

[25] M. Rahman, M. Zhao, M. S. Islam, K. Dong, and S. C. Saha, "Numerical study of nano and micro pollutant particle transport and deposition in realistic human lung airways," *Powder Technol*, vol. 402, p. 117364, Apr. 2022, doi: 10.1016/j.powtec.2022.117364.

[26] M. S. Islam, S. C. Saha, T. Gemci, I. A. Yang, E. Sauret, and Y. T. Gu, "Polydisperse Microparticle Transport and Deposition to the Terminal Bronchioles in a Heterogeneous Vasculature Tree," *Sci Rep*, vol. 8, no. 1, p. 16387, 2018, doi: 10.1038/s41598-018-34804-x.

[27] C. J. Musante, J. D. Schroeter, J. A. Rosati, T. M. Crowder, A. J. Hickey, and T. B. Martonen, "Factors Affecting the Deposition of Inhaled Porous Drug Particles," *J Pharm Sci*, vol. 91, no. 7, pp. 1590–1600, 2002, doi: https://doi.org/10.1002/jps.10152.

[28] X. G. Cui, E. M. Littringer, N. A. Urbanetz, and E. Gutheil, "LARGE EDDY SIMULATION OF POLYDISPERSE PARTICLE DEPOSITION IN AN IDEALIZED MOUTH-THROAT," *Atomization and Sprays*, vol. 28, no. 2, pp. 179–193, 2018, doi: 10.1615/AtomizSpr.2018025127.

[29] M. S. Islam *et al.*, "Euler-Lagrange Prediction of Diesel-Exhaust Polydisperse Particle Transport and Deposition in Lung: Anatomy and Turbulence Effects," *Sci Rep*, vol. 9, no. 1, p. 12423, 2019, doi: 10.1038/s41598-019-48753-6.

[30] E. R. Weibel, *Morphometry of the Human Lung*. Springer Berlin Heidelberg, 1963. doi: 10.1007/978-3-642-87553-3.

[31] Z. Zhang, C. Kleinstreuer, J. F. Donohue, and C. S. Kim, "Comparison of micro- and nano-size particle depositions in a human upper airway model," *J Aerosol Sci*, vol. 36, no. 2, pp. 211–233, 2005, doi: https://doi.org/10.1016/j.jaerosci.2004.08.006.

[32] A. D. Gosman and E. Ioannides, "Aspects of Computer Simulation of Liquid-Fueled Combustors," *Journal of Energy*, vol. 7, no. 6, pp. 482–490, Nov. 1983, doi: 10.2514/3.62687.

[33]   A. Li and G. Ahmadi, "Dispersion and Deposition of Spherical Particles from Point Sources in a Turbulent Channel Flow," *Aerosol Science and Technology*, vol. 16, no. 4, pp. 209–226, Jan. 1992, doi: 10.1080/02786829208959550.

[34]   P. G. Saffman, "The lift on a small sphere in a slow shear flow," *J Fluid Mech*, vol. 22, no. 2, pp. 385–400, 1965, doi: DOI: 10.1017/S0022112065000824.

[35]   "Ansys Fluent User's Guide," 2022. [Online]. Available: http://www.ansys.com

[36]   C. S. KIM, A. J. IGLESIAS, and L. GARCIA, "Deposition of Inhaled Particles in Bifurcating Airway Models: II. Expiratory Deposition," *Journal of Aerosol Medicine*, vol. 2, no. 1, pp. 15–27, Jan. 1989, doi: 10.1089/jam.1989.2.15.